ISTITUTO NAZIONALE DI FISICA NUCLEARE - ISTITUTO NAZIONALE DI FISICA NUCLEARE - ISTITUTO NAZIONALE DI FISICA NUCLEARE - ISTITUTO NAZIONALE DI FISICA NUCLEARE - ISTITUTO NAZIONALE DI FISICA NUCLEARE - ISTITUTO NAZIONALE DI

Laboratori Nazionali di Frascati

LNF-89/035(P)
31 Maggio 1989

L. Palumbo, V.G. Vaccaro:

WAKE FIELDS MEASUREMENTS

Invited talk presented at the
Joint US-CERN School on Particle Accelerators
"Frontiers of Particle Beams, Observation, Diagnosis and Correction"
Isola di Capri, Italy (20-26 October, 1988)

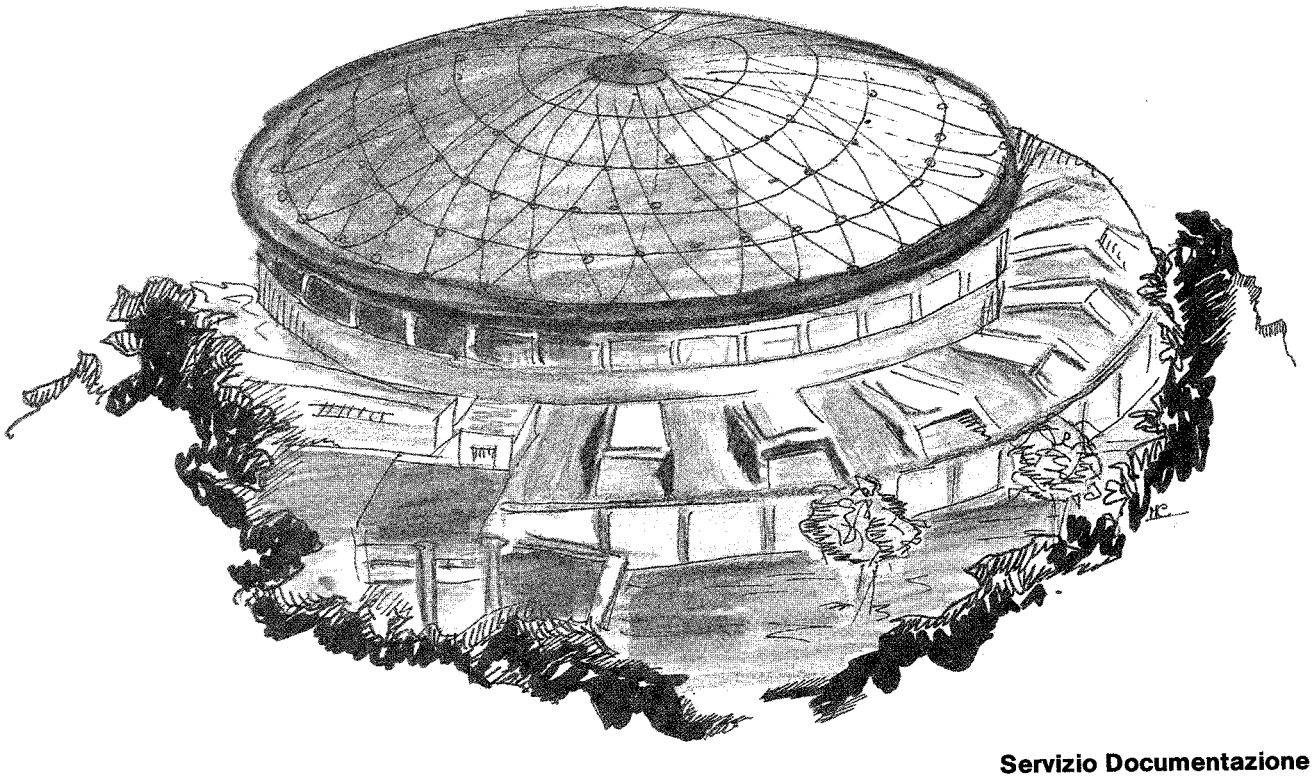

Servizio Documentazione
dei Laboratori Nazionali di Frascati
P.O. Box, 13 - 00044 Frascati (Italy)

INFN - Laboratori Nazionali di Frascati
Servizio Documentazione

LNF-89/035(P)
31 Maggio 1989

WAKE FIELDS MEASUREMENTS*

Luigi Palumbo
Dip. Energetica, Università di Roma "La Sapienza", and INFN - Laboratori Nazionali di Frascati, Italy.

Vittorio G.Vaccaro
Dip. Fisica, Università degli studi di Napoli, and INFN Sezione di Napoli, Italy.

TABLE OF CONTENTS

ABSTRACT

In this paper the concept of Wakefields and Machine Impedance are introduced. Several measurements techniques of these quantities either in the laboratory before installation or from beam observation are presented.

INTRODUCTION

The dynamics of an "ensemble" of charges in a linear or circular accelerating machine is affected by the so called "collective effects". These effects are generated by the electromagnetic forces, created by the interaction of the beam with the surrounding walls, which act back on the beam itself. The physical process is characterized by energy loss of the beam and, depending on the current intensity, by instability phenomena.

We may analyze the collective effects either in the time or in the frequency domain. The analysis in the time domain is usually adopted in the case of linear accelerators; the effects of the e.m. fields produced in the accelerating structure are described by means of the "Wake Potentials". For circular accelerators, due to the intrinsical periodicity of the structure, the analysis in the frequency domain is usually preferred; the e.m. fields are described in terms of the "Coupling Impedance" which is the image of the wake potential in the frequency domain (i.e. its Fourier transform).

We shall start this chapter by introducing the general definitions of Wake Potential and Impedance for both the longitudinal (parallel to trajectory) and transverse forces (Sec.1). Prediction and estimation of the above quantities are necessary for the assessment of the machine performances. Therefore, on one hand, there is a large effort in the theoretical analysis of the effect of all the machine elements (radiofrequency cavities, discontinuities, bellows etc.) in order to work out a reliable general model for the interaction beam-walls, while on the other hand, several measurement methods have been developed in order to verify the theoretical predictions and at the same time gather the information necessary for curing instabilities.

Measurement methods of the wake potential and of the coupling impedance are the subject of this chapter. We shall mainly deal with bench measurements of the wake potential (Sec.2) and measurement of the coupling impedance from beam observation (Sec.3).

1. LONGITUDINAL AND TRANSVERSE WAKE POTENTIALS

In this section we introduce the reader to the basic concepts and definitions of wake potentials showing some general properties and relationships. Examples of wake potentials for simple canonical structures can be found in Appendix [1-4] .

1.1 LONGITUDINAL WAKE POTENTIAL OF A POINT CHARGE

Let us consider two charges q_1 and q_2 travelling with constant velocity on the axis of an axially symmetric structure, and let their positions, at the time t = 0, be $z_1=0$ and $z_2 = -\beta c\tau$, where τ is the time delay of the trailing charge, see Fig.1. At any other instant "t" the leading and trailing charges have coordinates $z_1(t) = \beta c t$ and $z_2(t) = \beta c(t-\tau)$ respectively.

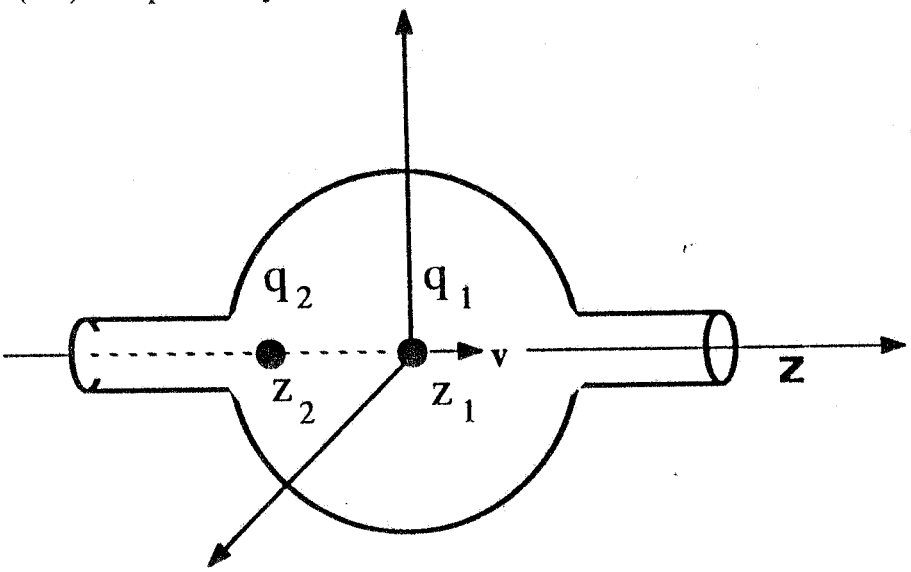

Fig. 1 Leading and trailing charges in a cavity with cylindrical symmetry

The electromagnetic fields **E** and **B** produced by the charge q_1 in the structure can be derived by solving the Maxwell equations satisfying proper boundary conditions.

The e.m. fields excited by q_1 can act back on the charge itself and on the trailing charge as well, affecting their dynamics. The Lorentz force

$$\mathbf{F} = q\left(\mathbf{E} + \mathbf{v} \times \mathbf{B}\right) \tag{1}$$

has in general a component along the z-axis and a component perpendicular to the trajectory. However, a charge moving on the axis of an axially symmetric structure produces on the axis only the longitudinal component E_z. Therefore the two charges experience only a longitudinal force which changes their energy. The energy lost by the charge q_1 over a flight distance *d* is :

$$U_{11} = - q_1 \int_d E_z \left(z, t = \frac{z}{\beta c} \right) dz \qquad (2)$$

Apart from particular cases of little interest, the quantity U_{11} is positive and takes account of the energy loss in the resistive walls and in the diffracted fields radiated by the charge encountering cross section variations in the surrounding pipe. The synchrotron radiated energy is usually dealt with separately as a single particle effect, although it could also be included in this treatment.

The trailing charge also changes its energy under the effect of the fields produced by the leading one :

$$U_{21} = - q_2 \int_d E_z \left(z, t = \frac{z}{\beta c} - \tau \right) dz \qquad (3)$$

where the electric field is computed at a time with delay τ. The quantity U_{21} is a function of this delay and can in general be positive (energy loss) or negative (energy gain).

We define **loss factor k** the energy lost by q_1 per unit charge:

$$k = \frac{U_{11}}{q_1^{\,2}} \qquad (4)$$

and **wake potential** $w(\tau)$ the energy lost by q_2 per unit of both charges q_1 and q_2:

$$w(\tau) = \frac{U_{21}}{q_1 \, q_2} \qquad (5)$$

Thus the wake potential is a close relative of the loss factor and is given in the same units (**Volt/Coulomb**). We also find in the literature the denomination "wake function" sometimes with the specification "impulsive" because of the point charge origin of the fields.

The reader could argue from the above definitions that the loss factor is equal to the wake potential in the limit of zero time delay ($\tau = 0$). This result is not true, and it has been proved that the exact relation is [2]:

$$k = \frac{w\,(\tau = 0)}{2} \qquad (6)$$

An intuitive explanation of it will be given in the next paragraph concerning general charge distributions.

There is an important behavior of the wake potential worth mentioning. Due to the finite propagation velocity of the induced fields and to the motion of the source charge, the wake potential is, in general, not symmetric with respect to

the charge position. For the limit case of a charge with light velocity it exists only in the region $z < c\tau$, while it vanishes elsewhere. This property is a consequence of the causality principle [2,3].

The wake potential defined so far is useful for studying the longitudinal dynamics of a charged particle starting from its potential in the e.m. fields, given by the wake times the charge of the particle. However, sometimes, it can be convenient to use the equation of the motion in terms of the force acting on the particle; the average force experienced by a charge q_2 is :

$$\langle F_z(\tau) \rangle = \frac{- q_1 q_2 w(\tau)}{d} \tag{7}$$

1.2 LONGITUDINAL WAKE OF A CHARGE DISTRIBUTION

Assume now that the charge q_1 is continuously distributed over the z-axis according to the time distribution function $I(\tau)$ such that:

$$q_1 = \int_{-\infty}^{\infty} I(\tau)\, d\tau \tag{8}$$

What is the wake potential produced by the distribution at a point with time delay τ ? The answer is found by applying the superposition principle, splitting the distribution into an infinite number of infinitesimal slices (Fig. 2) and adding their wake contributions. According to the definitions given in the previous paragraph, the energy lost by the charge q_2 experiencing the wake produced by the slice in τ' is:

$$dU_{21}(\tau - \tau') = q_2\, I(\tau')\, d\tau'\, w\,(\tau - \tau') \tag{9}$$

and summing all the effects we get the wake potential per unit charge of a bunch distribution as:

$$W_b(\tau) = \frac{U_{21}}{q_1\, q_2} = \frac{1}{q_1} \int_{-\infty}^{\infty} w\,(\tau - \tau')\, I(\tau')\, d\tau' \tag{10}$$

For a bunch travelling with velocity c, because of the causality, the above folding integral has the observation point τ as uppermost limit.

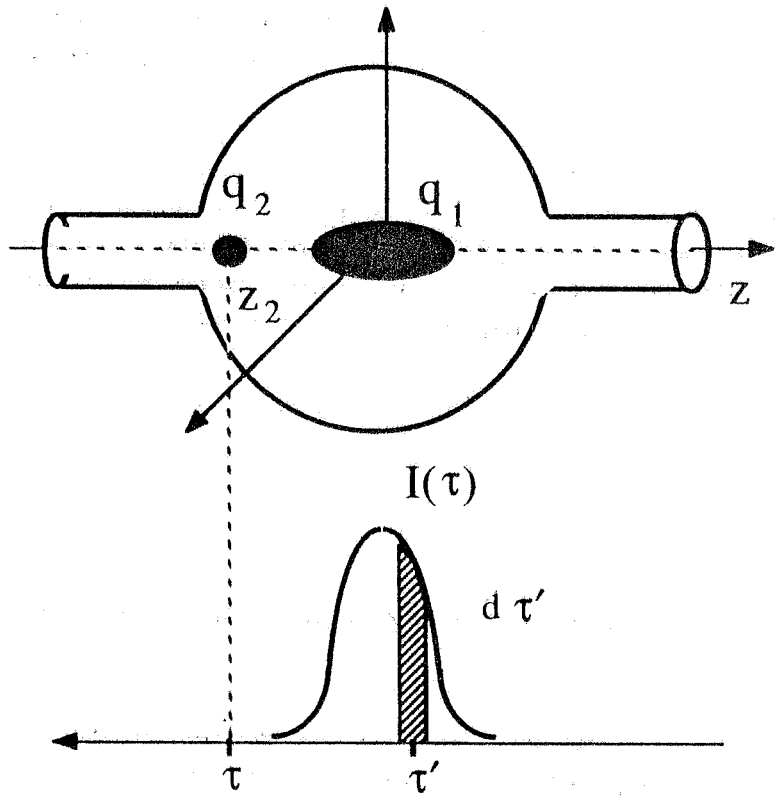

Fig. 2 Continuous charge distribution.

The losses correspond to an average force experienced by q_2 given by:

$$\langle F_z(\tau) \rangle = \frac{- q_1 q_2 W_b(\tau)}{d} \tag{11}$$

Once the wake potential $W_b(\tau)$ is known it is straightforward to derive the loss factor of the charge distribution by applying again the superposition principle; we get:

$$k = \frac{U_{11}}{q_1^{\,2}} = \frac{1}{q_1} \int_{-\infty}^{\infty} W_b(\tau)\, I(\tau)\, d\tau \tag{12}$$

Assume now that the bunch is so short that it can be considered as two half-charges very close to each other at $\tau = 0$. Each half-charge loses individually the energy $[(q/2)^2\ k]$, but the second half-charge, because of the wake produced by the first one, loses an additional quantity of energy $[(q/2)^2\ w(\tau = 0)]$. The total energy lost must be equal to the energy lost by a single charge q in the limit of zero distance between the two half-charges $[q^2 k]$, obtaining the simple relation previously shown:

$$k = \frac{w\ (\tau = 0)}{2} \tag{13}$$

1.3 TRANSVERSE WAKE POTENTIAL OF A POINT CHARGE

Let us consider now the leading charge transversely displaced with respect to the axis as shown in Fig. 3. The charge excites in the structure electromagnetic fields which can be expanded in their multipolar components (dipole, quadrupole, sextupole etc.) in the transverse plane. For small displacements the dipole term is of course dominant. However, the analysis of these components is sometimes developed up to the sextupole term (the first significant non-linear term). We shall limit ourselves to the transverse effects of the dipole term only.

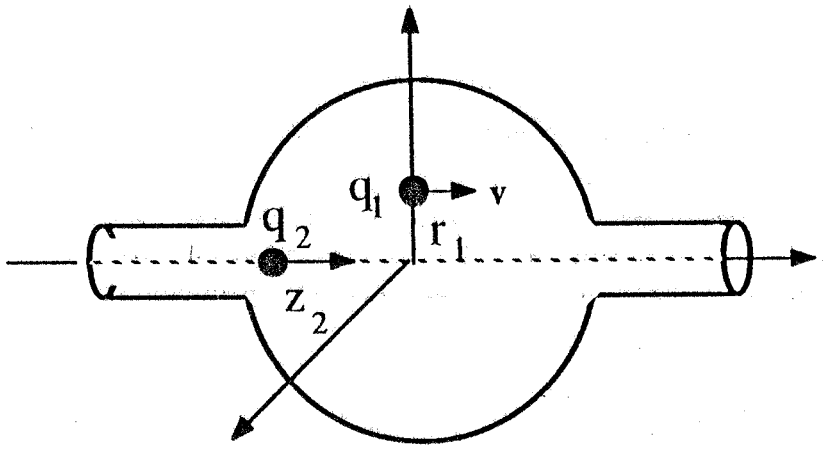

Fig. 3 The leading charge is transversely displaced

The charge q_2 experiences a Lorentz force which has longitudinal and transverse components. The longitudinal dipole force induces a longitudinal dipole wakefield which can be taken into account in the same way as shown in Sec.1.1; however, for small displacements, it represents only a negligible correction to the longitudinal wake produced by the charge on the axis. The transverse dipole force is parallel to the charge displacement (this is true only in the case of axially symmetric structure).

The trailing charge receives a transverse momentum kick over a distance d given by:

$$M(\tau) = q_2 \int_d \left[\mathbf{E}(z,t) + \mathbf{v} \times \mathbf{B}(z,t)\right]_\perp dz \; ; \quad \text{with } t = \frac{z}{\beta c} - \tau \tag{14}$$

directed along r_1 because of the axial symmetry. The amplitude of this transverse kick per unit of both charges and per unity transverse displacement defines the **transverse wake potential** of a point charge:

$$w_\perp(\tau) = \frac{M(\tau)}{q_1 q_2 r_1} \tag{15}$$

expressed in (**Volt/Coulomb Meter**) units. In the limit case of charges with light velocity, the transverse wake does not depend on the transverse position of the trailing charge and exists only in the region behind the leading charge. However, for more general cases this simple scalar approach is not valid, and the transverse wake is better represented as a dyadic operator [1].

The average transverse force experienced by the trailing charge over a distance d is :

$$\left\langle \mathbf{F}_{\perp}(\tau) \right\rangle = \frac{q_1 q_2 w_{\perp}(\tau)}{d} \mathbf{r}_1 \tag{16}$$

1.4 TRANSVERSE WAKE POTENTIAL OF A CHARGE DISTRIBUTION

Analogously to the longitudinal case, the transverse wake potential (per unit charge) produced by a continuous bunch distribution, transversely displaced of r_1, can be obtained by applying the superposition principle; we get:

$$W_{b\perp}(\tau) = \frac{M(\tau)}{q_1\ q_2 r_1} = \frac{1}{q_1} \int_{-\infty}^{\infty} w_{\perp}(\tau - \tau')\, I(\tau')\, d\tau' \tag{17}$$

The transverse average force acting on a charge q_2 within the bunch is therefore:

$$\left\langle \mathbf{F}_{\perp}(\tau) \right\rangle = \frac{M(\tau)}{d} = \frac{q_1 q_2 W_{b\perp}(\tau)}{d} \mathbf{r}_1 \tag{18}$$

1.5 LONGITUDINAL COUPLING IMPEDANCE

In the frequency domain we compute the Fourier spectrum of the point charge wake potential [1-5]:

$$\mathcal{F}\left[w(\tau)\right] = \frac{1}{2\pi} \int_{-\infty}^{\infty} w(\tau)\, e^{-j\omega\tau}\, d\tau \equiv Z(\omega) \tag{19}$$

which is called **Coupling Impedance** because it turns out to have **Ohms** units. The wake potential is derived from the impedance by inverting the Fourier integral:

$$w(\tau) = \mathcal{F}^{-1}\left[Z(\omega)\right] = \int_{-\infty}^{\infty} Z(\omega)\, e^{j\omega\tau}\, d\omega \qquad (20)$$

The coupling impedance is a complex quantity:

$$Z(\omega) = Z_r(\omega) + j\, Z_i(\omega) \qquad (21)$$

Since w(t) is a real function it is easy to prove that, with respect to the frequency, $Z_r(\omega)$ is an even function while $Z_i(\omega)$ is an odd function. Recalling the relation between loss factor and wake potential for a point charge, Eq. (5), it is also easy to find that the real part of the impedance is the power spectrum of the energy loss of a unit point charge:

$$k = \frac{w(\tau=0)}{2} = \int_0^{\infty} Z_r(\omega)\, d\omega \qquad (22)$$

In the case of a charge distribution $I(\tau)$, whose Fourier spectrum is $I(\omega)$, the total wake potential $W_b(\tau)$ and the loss factor may be expressed in terms of $Z(\omega)$ by transforming the integrals (10) and (12), obtaining:

$$W_b(\tau) = \frac{1}{q_1} \int_{-\infty}^{\infty} Z(\omega)\, I(\omega)\, e^{j\omega\tau}\, d\omega \qquad (23)$$

$$k = \frac{1}{q_1^2} \int_{-\infty}^{\infty} Z_r(\omega) \left|I(\omega)\right|^2 d\omega \qquad (24)$$

while the average force experienced by a single charge q_2 within the distribution is [6,9]:

$$\left\langle F(\tau)\right\rangle = \frac{-q_1 q_2 W_b(\tau)}{d} = \frac{-q_2}{d} \int_{-\infty}^{\infty} Z(\omega)\, I(\omega)\, e^{j\omega\tau}\, d\omega \qquad (25)$$

As an example consider a gaussian bunch distribution q_2 with standard deviation σ_τ, we have:

$$I(\omega) = \frac{q_1}{2\pi}\, e^{-\frac{1}{2}\left(\omega\sigma_\tau\right)^2} \qquad (26)$$

and therefore the loss factor is given by:

$$k(\sigma_\tau) = \frac{1}{\pi}\int_0^\infty Z_r(\omega)\, e^{-(\omega\sigma_\tau)^2}\, d\omega \qquad (27)$$

It is apparent that the loss factor is, in general, a function of the r.m.s. duration of the bunch distribution. It is interesting to note that there exists a general relation, useful in the measurements, between the frequency dependence of the impedance and the dependence of the loss factor on the bunch length:

$$Z_r(\omega) \propto \omega^a \quad \Leftrightarrow \quad k(\sigma_\tau) \propto \left(\frac{1}{\sigma_\tau}\right)^{a+1} \qquad (28)$$

1.6 TRANSVERSE COUPLING IMPEDANCE

The Fourier transform of the transverse wake in the frequency domain times the imaginary unity defines the transverse coupling impedance:

$$\mathcal{F}\left[w_\perp(\tau)\right] = \frac{j}{2\pi}\int_{-\infty}^{\infty} w_\perp(\tau)\, e^{-j\omega\tau}\, d\tau \equiv Z_\perp(\omega) \qquad (29)$$

which has **Ohms/Meter** units. Accordingly the transverse wake is obtained by means of the inverse Fourier transform of the transverse impedance:

$$w_\perp(\tau) = \mathcal{F}^{-1}\left[Z_\perp(\omega)\right] = -j\int_{-\infty}^{\infty} Z_\perp(\omega)\, e^{j\omega\tau}\, d\omega \qquad (30)$$

Analogously to the longitudinal case we may express the transverse wake per unit charge of a charge distribution q_1, and the average transverse force experienced by q_2, as [6-9]:

$$W_{b\perp}(\tau) = \frac{-j}{q_1}\int_{-\infty}^{\infty} Z_\perp(\omega)\, I(\omega)\, e^{j\omega\tau}\, d\omega \qquad (31a)$$

$$\left\langle F_\perp(\tau)\right\rangle = \frac{q_1 q_2 W_{b\perp}(\tau)}{d} r_1 = -j\frac{q_2 r_1}{d}\int_{-\infty}^{\infty} Z_\perp(\omega)\, I(\omega)\, e^{j\omega\tau}\, d\omega \qquad (31b)$$

2. MEASUREMENTS IN LABORATORY BEFORE INSTALLATION

The methods developed for measuring the wake potentials are mainly concerned with accelerating r.f. cavities, the basic constituent of linear accelerators. In general we may group the measurements in two categories: direct and indirect measurements.

2.1 DIRECT MEASUREMENT OF THE WAKE POTENTIALS

The direct measurement of the longitudinal wake potential appears to be relatively simple in principle. In fact one has to inject two charged particles (with variable time distance) in a given structure and observe the energy change of the trailing charge due to the e.m. fields produced by the leading one. However, a single elementary charge is unlikely to induce a detectable change of energy, so that it is necessary to use intense bunches of particles which in turn are difficult to concentrate in very small volumes. Therefore, in practice, we can observe only the wakefield effects relative to charge distributions; obviously the shorter is the bunch the more the measured wake approaches the impulsive wake potential.

To this end a test facility has been built at Argonne [10], where two bunched beams of different energy and intensity have been used; the change of energy of the trailing bunch (low intensity and energy) is mainly due to the effect of the wake fields because its own losses are negligible. The two bunches pass through the test r.f. structure with adjustable delay ending their flight in a spectrometer (Fig. 4) where it is possible to measure their energies, the beams' current, their dimensions and positions.

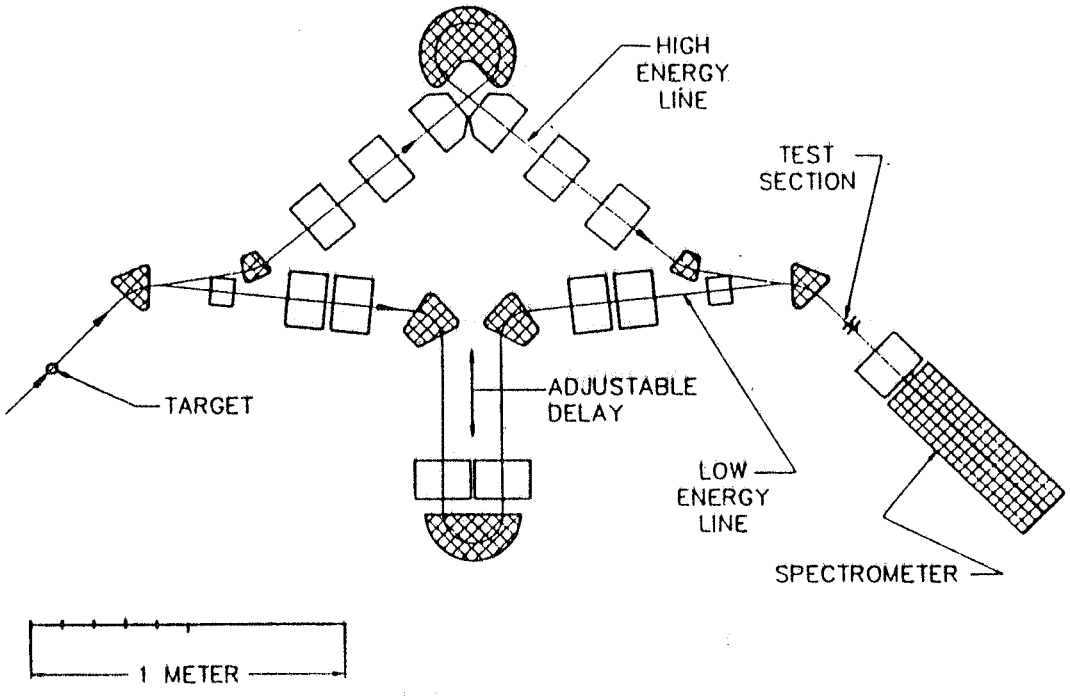

Fig. 4 The Argonne test facility [10] for wake potential measurement.

The energy change of the trailing bunch per unit of both charges gives directly the longitudinal wake potential of the structure. The transverse wake is not measured directly, but can be derived by observing the transverse displacement of the trailing bunch center caused by an off-axis injection of the leading one. Results of the longitudinal wake and transverse displacement are reported in Figs. 5a and 5b. The wake is produced by a bunch of duration σ_τ.

The energy gain of the trailing bunch is :

$$\Delta U(\tau) = 2\, q_1 q_2 \sum_n k_n \exp\left[-\frac{1}{2}(\omega_n \sigma_\tau)^2\right] \cos(\omega_n \tau)$$

Due to the non-negligible bunch dimensions, the energy gain of the trailing charge and its transverse displacement are strongly dominated by the fundamental mode of the resonant structure.

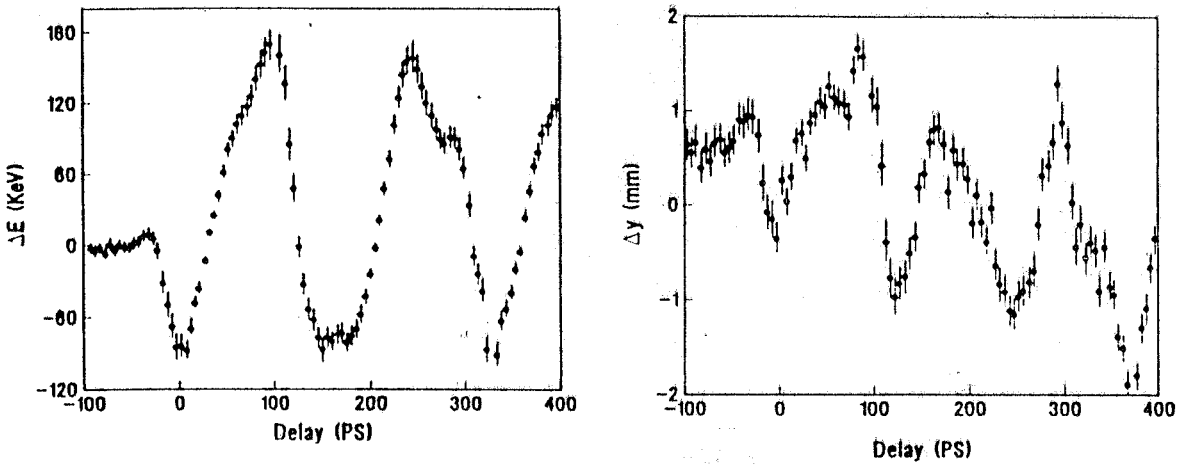

Fig. 5 Energy loss and transverse test bunch displacement.

2.2 PERTURBATION METHOD

The wake potential of a resonant structure is uniquely determined if the infinite set of its normal resonant modes ω_n is known together with the quality factor Q_n and the ratio $(R/Q)_n$ of each mode (see Appendix). All these quantities can be measured using standard microwave techniques [11,12,13]. Here we shall briefly describe the perturbation method commonly used to derive $(R/Q)_n$ which is defined for the monopole mode as:

$$\left(\frac{R}{Q}\right)_n = \frac{1}{\omega_n U_n}\left|\int_0^L E_z(z)\, e^{j\omega_n z/c} dz\right|^2 \qquad (32)$$

and for the dipole deflecting mode as:

$$\left(\frac{R}{Q}\right)_{n\perp} = \left(\frac{c}{\omega_n\, b}\right)^2 \frac{1}{\omega_n U_n} \left| \int_0^L E_z(z)\, e^{j\omega_n z/c} dz \right|^2 \qquad (33)$$

where L is the resonant structure length, the electric field is evaluated on the cavity axis for the monopole mode and on the path at the distance b (cavity iris radius) parallel to the axis for the dipole modes.

A precise estimation of this quantity can be achieved by measuring the longitudinal electric field on the axis (normalized to the stored energy) by means of the Frequency Perturbation Method (FPM) proposed by J.C. Slater in 1946 [11,12]. The Slater theorem expresses quantitatively the frequency shift occurring in a resonant cavity when the boundary conditions are slightly perturbed by the introduction of small objects in the cavity, or by compression (depression) of the external cavity walls.

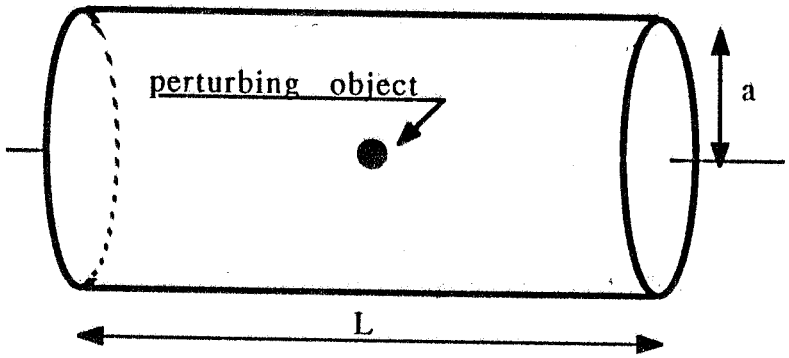

Fig. 6 Pill box cavity with a perturbing object

It is well known that at resonance the same quantity of energy is stored in the electric and magnetic fields, and that the resonant frequency depends on the cavity geometry and on the e.m. properties of the cavity walls and of the matter filling the cavity. It is then intuitive that a modification of the boundary conditions modifies the energy balance and therefore makes the resonant frequency shift to where the energy balance is restored. If we introduce in the cavity a small conducting object (Fig. 6), we observe a frequency shift given by:

$$\frac{\Delta f}{f_0} = \frac{\int_{Vol} \left(\mu H_0^2 - \varepsilon E_0^2\right) dV}{U} \qquad (34)$$

We can recognize the numerator of the rhs as the difference between the magnetic and electric energies of the unperturbed fields stored in the small volume where the perturbing object is placed. Since the electric and magnetic

fields vanish inside the conductor, one can speak of energies "subtracted" by the perturbing object. This statement is absolutely true only for perfectly conducting objects, otherwise there is penetration of fields due to the skin effect. However this effect is negligible when the object size is small compared to the field wavelength and one can use the static approximation.

Example

A simple example of the application of this theorem can be given by considering the pill-box cavity of Fig. 6. Assuming that the TM_{010} is the fundamental mode, the field components are:

$$\begin{cases} E_z = E_0 J_0\left(\frac{\nu_{01} r}{a}\right) \cos(\omega_0 t) \\ H_\phi = -\frac{E_0}{Z_0} J_1\left(\frac{\nu_{01} r}{a}\right) \sin(\omega_0 t) \end{cases} \tag{35}$$

where $Z_0 = 377\ \Omega$, the resonant angular frequency is :

$$\omega_0 = \frac{c\nu_{01}}{a} \tag{36}$$

and ν_{01} is the first zero of the Bessel function $J_0(x)$.

The average energy stored in the fundamental mode is given by the sum of equal contributions, i.e. the energy stored in the electric and magnetic fields:

$$U = U_E + U_M = \varepsilon_0 \left\langle \int_{Vol} E^2 \, dV \right\rangle = \frac{\pi}{2} \varepsilon_0 E_0^2 L a^2 J_1^2(\nu_{01}) \tag{37}$$

If we apply a light compression to the lateral cylindrical surface so as to decrease the pipe radius to (a - Δa), the relative increase of resonant frequency is given by $\Delta\omega/\omega_0 \approx \Delta a/a$. We note now that the volume change occurs in a region where the electric field is zero (the fundamental mode has only the z-component), therefore there is only a magnetic energy subtraction given by:

$$\Delta U_M = \frac{\pi}{2} \varepsilon_0 E_0^2 L a J_1^2(\nu_{01}) \Delta a \tag{38}$$

which, divided by the unperturbed total energy U, gives exactly the relative frequency shift.

Now that we have gained insight in the Slater theorem, let us see how is it used to derive informations on the fields.

In principle we may use a conducting object of any size and shape. However simple relationships between the "subtracted" energy and the unperturbed local

fields can be established by considering conducting objects of particular symmetry (needles, disks, spheres) and of size smaller than the wavelength of the resonant mode. In this case, in fact, we are allowed to solve the Maxwell equations inside the object using the static approximation, and simple expressions of Eq.(34) can be derived. Accordingly the resonant frequency shift produced by a symmetric perturbing object is related to the local fields by:

$$\frac{\Delta f}{f_0} = \frac{\varepsilon_0\left(K_1 E_{//}^2 + K_2 E_{\perp}^2\right) - \mu_0\left(K_3 H_{//}^2 + K_4 H_{\perp}^2\right)}{U} \tag{39}$$

where the field's components parallel (//) and perpendicular ($\perp$) to the object's main axis of the perturbing object contribute to the frequency shift depending on the form factors K_i (i=1,4) whose expressions have to be derived for each particular shape.

Needles perturb only the parallel component of the electric field and are the ideal perturbing objects for our purposes. Unfortunately a precise evaluation of the form factor K_1 has been worked out only for a thin ellipsoid of revolution which, being very difficult to manufacture, yields large measurement errors. Only recently the form factor of a hollow thin cylinder (much simpler to make) has been calculated [15] with a good precision allowing this object to be used instead of a small sphere in the field strength measurements.

Spheres perturb both electric and magnetic fields independently of a particular orientation so that they are characterized only by two form factors [12]:

$$K_1 = K_2 = 3V$$
$$K_3 = K_4 = \frac{3}{2}V \tag{40}$$

where V is the sphere volume. They are commonly used for measuring the field's strength on the cavity axis, i.e in a region where, because of the symmetry, there is only the electric field. The scheme of the experimental set-up used by Slater and Maier in 1952 is shown in Fig. 7. The test object was displaced by means of a silk thread connected to a mechanical position recorder. The feeder, klystron-1, is locked to the resonant frequency of the cavity perturbed by the metallic bead, while a second klystron oscillates at the unperturbed frequency of the natural cavity mode under observation, previously measured. The signals of the two klystrons are then mixed and filtered via an AM receiver which shows only the beat wave signal whose frequency is equal to the frequency shift.

Nowadays the measurement technique has not changed so much in its principles, but the replacement of the mechanical displacement system with a controlled stepping motor, and the use of digital network analyzers, the whole system being controlled by computers, allows short measurement time and high precision , see for example Ref. [14].

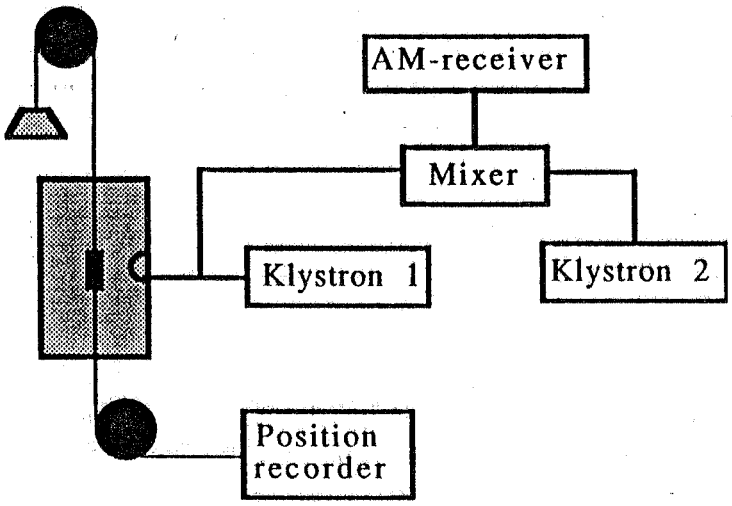

Fig. 7 Scheme of measurement by Slater and Maier

It is worth mentioning the measurement set-up shown in Fig. 8, where the perturbed frequency is obtained by measuring the phase of a signal from the cavity, at the unperturbed frequency (phase shift method) [15].

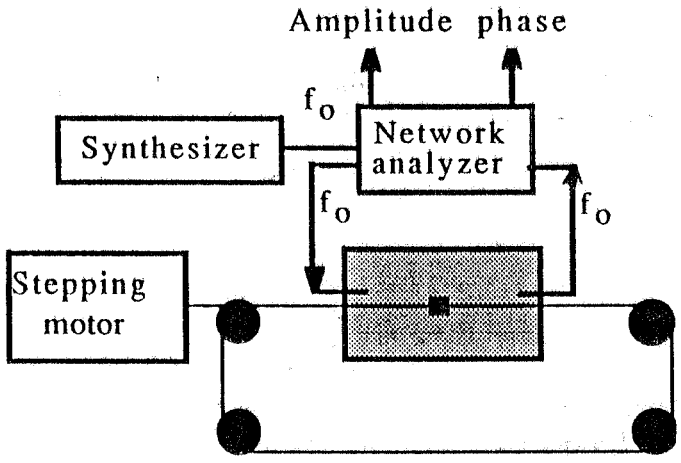

Fig. 8 Phase shift measurement method

The main advantage of this method is its intrinsical simplicity allowing fast measurements. The probe exciting the cavity and the probe detecting the output signal are adjusted for a very weak coupling by two (input and output) high gain amplifiers (30 dB), yielding a negligible change of the merit factor ($Q_{loaded} \cong Q_{unloaded}$). The amplitude ratio of the transmitted signal (the transmission coefficient S_{21}) is used to determine the resonant frequency f_o with an accuracy of 10^{-3}. A cylindrical needle, whose form factor has been accurately calculated, is used as perturbing object while the frequency shift is obtained by measuring the phase ϕ of the transmitted signal at f_o:

$$\frac{f - f_o}{f_o} = \frac{1}{Q_{load}} tg\,\phi \qquad (41)$$

the quality factor can be estimated from phase measurement using the ±45° bandwidth method or by evaluating the phase slope variation $|\partial\phi/\partial\omega|_{\omega=\omega r}$ at resonance.

The main disadvantages, compared with the direct frequency method, are:

- considerable errors may result in the evaluation of R/Q, due to the non linearity of Eq. (41), expecially if the resonant frequency is not evaluated with high precision; this also limits the amplitude of the perturbation and therefore the overall sensitivity;

- at the points where the field is weak, the resulting phase shift can be too small to be detected independently of the amplitude of the feeding signal. In the direct method the noise may be reduced by using large r.f. signals.

Errors common in both methods are caused by:

- the thread and the probes themselves causing a frequency shift;

- temperature drift;

- for long horizontal r.f. structures, the catenary drop of the thread causes a transverse displacement of the perturbing object.

It is worth remarking that the frequency or phase shift methods are simple to apply as long as the perturbing object size is small compared to the field's wavelength. On the other hand the bead size cannot be reduced beyond a value imposed by the measurement sensitivity so that the range of applicability of the methods is limited to a low number of high order modes (HOM). A new type of perturbing object developed to increase the sensitivity and therefore the maximum number of HOM is described in Ref. [16].

Finally it must be mentioned, to complete this subject, that a shift of the resonant frequency can also be caused by the insertion of dielectric or ferromagnetic objects:

$$\frac{\Delta f}{f_0} = - \frac{\int_{Vol} \left(\Delta\mu H_0^2 + \Delta\varepsilon E_0^2\right) dV}{U} \qquad (42)$$

While with a conducting body the resonant frequency can increase or decrease depending on the prevalence of electric or magnetic energy reduction, it can only decrease by introducing dielectric or ferromagnetic materials. A useful property of these objects is that, in contrast to conducting ones, they act separately on the electric and magnetic fields. An interesting application of dielectric beads for measurements of longitudinal and transverse impedance can be found in Ref. [17].

2.3 BENCH MEASUREMENT OF ENERGY LOSS AND WAKE POTENTIAL

This method was proposed by M. Sands and J. Rees [18] in 1974 for the measurement of the energy loss of a stored beam to a cavity due to the higher-mode excitation. They argued that the energy lost by a short current pulse on a central wire is the same as that lost by a bunch of particles having equal time shape.

A bunch of particles passing through the cavity excites secondary fields (wake-fields) qualitatively sketched in Fig. 9. These fields acting back on the bunch change the energy of each particle according to Eq. (10):

$$U(\tau) = qe\, W_b(\tau) \tag{43}$$

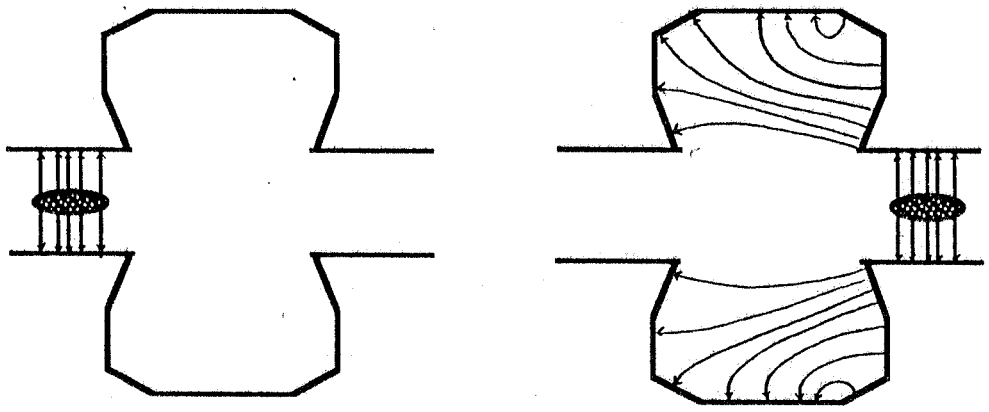

Fig. 9 Qualitative behaviour fields excited by a bunch in a cavity

The total energy lost by the bunch is given by Eq. (12)

$$U_{tot} = q \int_{-\infty}^{\infty} W_b(\tau)\, I(\tau)\, d\tau \tag{44}$$

A short current pulse transmitted along a thin axial wire simulates a relativistic particle bunch. The basic idea of the method is that if the duration of the beam pulse is short compared to the relaxation time of the fields in the cavity, then the energy removed from the pulse is similar to the energy lost by the bunch. The presence of the wire modifies the time evolution of the fields after the passage of the pulse, Fig. 10, but not the total energy stored in the fields excited in the cavity. In fact in presence of the wire these fields instead of reflecting back and forth in the cavity (generating the resonant modes), flow outward by coupling to the coaxial line.

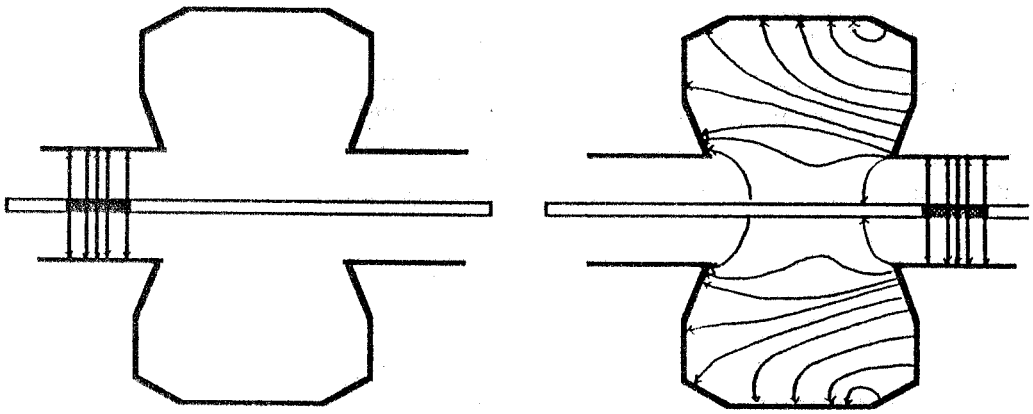

Fig. 10 Fields excited by a current pulse on a central wire

The problem therefore reduces to developing a method for measuring the energy removed from the pulse. The experimental arrangement proposed in Ref. [18] is shown in Fig.11.

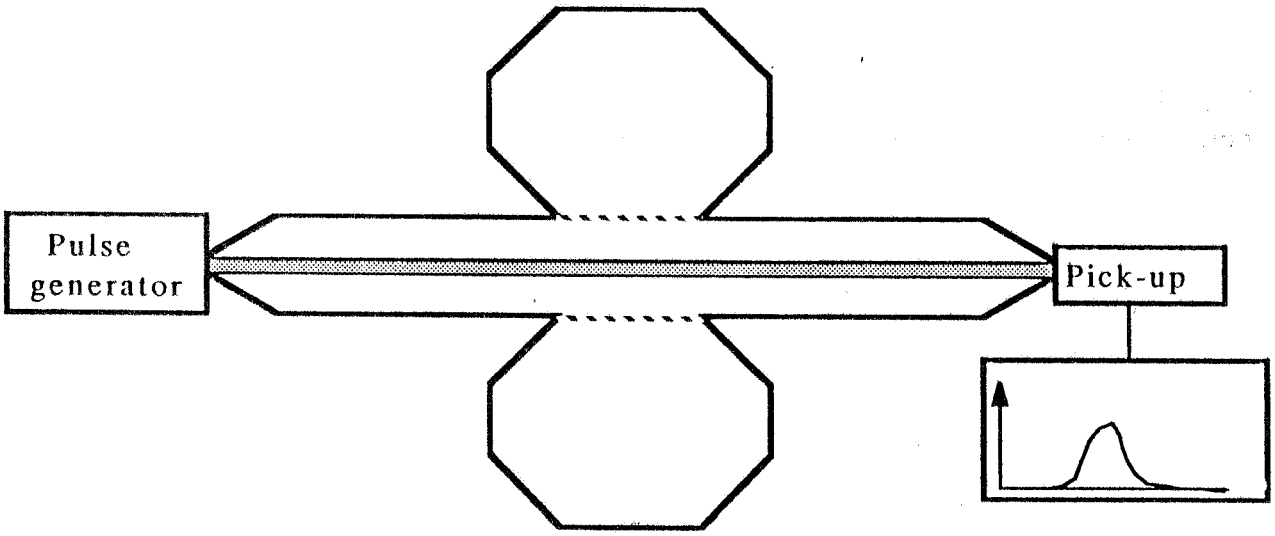

Fig. 11 Experimental scheme for measurement of the energy lost by a current pulse

It consists of a narrow pulse generator generally producing rectangular pulses. The pulse is filtered in a pulse shaping network to produce a Gaussian shape and then sent, through a tapered section, to a coaxial structure which ends with a second tapered section, coupling the output pulse to the detector head of a sampling oscillograph. The role of the tapers is to mantain the characteristic impedance constant.

Firstly a current pulse $i_1(t)$ is fed into a simple, matched, coaxial structure with characteristic impedance $R_0 = (Z_0/2\pi)\ln(b/a)$, where a and b are the wire and pipe

radii respectively. The signal travels along the coaxial line without reflection, and its time shape is recorded at the coaxial line end. Since the pulses are very short (hundreds of picoseconds) the use of the sampling technique is mandatory and many identical pulses have to be generated. The energy contained in the pulse can be evaluated at any point of the coaxial line as:

$$U_1 = \int_{-\infty}^{\infty} R_0 \, i_1^2(t) \, dt \tag{45}$$

An identical pulse is then fed into the structure with the testing object (for example a cavity) replacing part of the coaxial line. Let $i_2(t)$ be the time dependence of the perturbed transmitted pulse recorded by the sampling oscillograph. The energy contained in this pulse downstream of the cavity can be evaluated in the same way as for the unperturbed pulse. Assuming that the pulse is only slightly modified, i.e. $i_2(t) = i_1(t) + \Delta i(t)$, the energy contained in the perturbed pulse can be written as:

$$U_2 = \int_{-\infty}^{\infty} R_0 \, i_1^2(t) \, dt + \int_{-\infty}^{\infty} 2R_0 \, i_1(t) \, \Delta i(t) \, dt + \int_{-\infty}^{\infty} R_0 \, \Delta i^2(t) \, dt \tag{46}$$

The difference between expressions 45) and 46) gives the energy lost by the current pulse. In the case of small perturbations, i.e. if

$$\left[\frac{|\Delta i(t)|}{i_{1\,max}} \right] << 1 \tag{47}$$

the energy lost by the pulse is given by:

$$U = U_1 - U_2 = - \int_{-\infty}^{\infty} 2R_0 \, i_1(t) \, \Delta i(t) \, dt \tag{48}$$

The above integral extends in practice only over a limited time range. Comparing it to the expression of the energy loss of a bunch of particles, Eq.(12) , we can derive that the signal difference $\Delta i(t)$ times $(-2R_0/q)$ equals the wake potential of a bunch of particles with the same time shape:

$$W_b(\tau) = - \frac{2R_0}{q} \, \Delta i(t) \tag{49}$$

The better inequality (47) is satisfied, the higher is the coaxial-wire impedance, which implies the use of very thin wires. However the wire radius cannot be chosen to be infinitely thin [18,23], the main reason being the almost disappearance of the difference signal $\Delta i(t)$, which would lead to large errors in the wake estimation.

The wire method requires a high accuracy in the evaluation of the quantity

$\Delta i(t)$. To this end it is necessary that identical pulses be generated with high precision, and the whole measuring system be stable. It is therefore convenient to use two separate parallel branches containing the normal pipe and the test object (see for instance Ref. [19]).

An interesting application of the method can be found in Ref. [20] together with a comparison between the measured and computed loss.

Transforming Eq.(49) into the frequency domain yields:

$$Z(\omega)I_1(\omega) = -2R_0\left[I_1(\omega) - I_2(\omega)\right] \tag{50}$$

which relates the complex coupling impedance to the (complex) current's spectra. It is worth noting that the ratio $Z(\omega)/2R_0$ is the same as $\Delta I(\omega)/I_1(\omega)$ and therefore, because of Eq. (47), must be acceptably small.

High precision measurements may be performed directly in the frequency domain [21,22] by adopting the experimental arrangement shown in Fig.13.

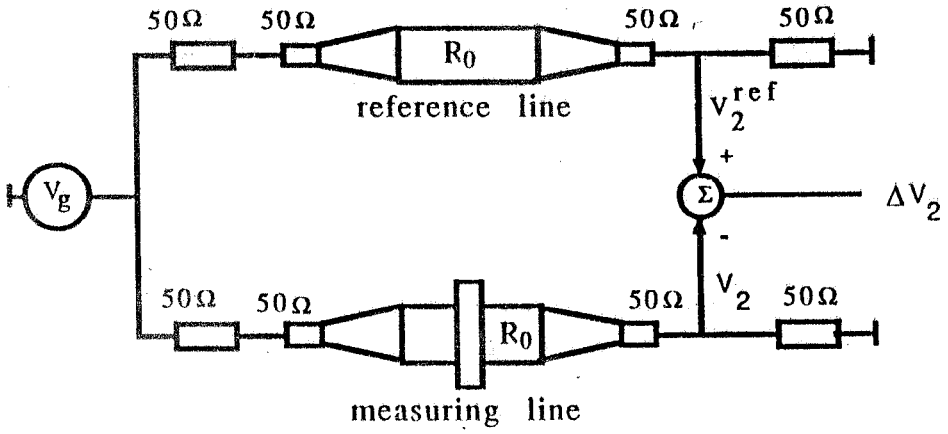

Fig. 13 Synthetic pulse measurement (frequency domain)

According to Eq.(50) the longitudinal coupling impedance is given by:

$$Z(\omega) = 2\,R_0\,\frac{\Delta V_2}{V_2^{ref}} \tag{51}$$

3. IMPEDANCE MEASUREMENTS FROM BEAM OBSERVATION

INTRODUCTION

So far we have dealt with several methods used in the measurement of the wakefields or impedances of individual vacuum chamber components such as cavities, bellows, kickers etc, before their installation.

A point charge travelling in a real machine experiences the effects of all vacuum chamber components. In the frequency domain these effects simply add at frequencies below the lowest cutoff of the beam pipe, while at higher frequencies mutual effects among various elements, due to the field propagation within the beam pipe, should be considered.

The longitudinal and transverse dynamics of charged bunches are affected by these fields. Analysis of the beam dynamics in the frequency domain shows that instability thresholds and growth rates depend on the machine impedances. In particular one finds that the resistive part is responsible for parasitic energy losses and growth rates of instabilities, while the reactive part causes frequency shifts and potential-well distortions [2,5-9]. Observation of these effects is a powerful means for machine physicists to deduce the machine impedance.

Descriptions of all the beam observation methods related to impedance measurements would need much more space than allowed here. Therefore only a few basic measurements, concerning mainly the single bunch dynamics, will now be described. These measurements have been performed on almost all the existing machines and it is impossible to cite all of them.

3.1 MACHINE IMPEDANCE

The coupling impedance of a real accelerating structure is quite complex. It is the result of several contributions: space charge, resistive walls, parasitic modes of resonant structures, discontinuities of the vacuum chamber, etc, each with a different frequency and energy dependence. A qualitative frequency behaviour is shown in Fig. 14.

According to Eqs. (10) and (17), the longitudinal and transverse forces acting on the bunch depend on the bunch spectrum. The bunch spectrum behaves like a filter so that only a limited frequency region of the impedance affects the beam dynamics. Therefore by monitoring, for instance, long bunches only the low frequency part of the impedance can be probed.

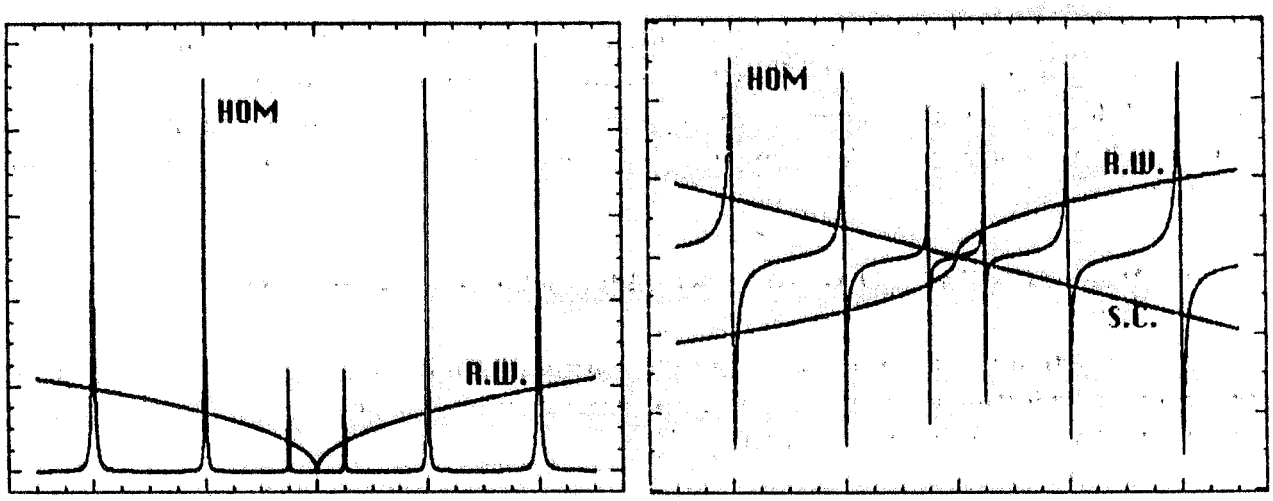

Fig. 14 Machine impedance : a) Resistive. b) Inductive.

Moreover, in the study of the single-bunch dynamics, one finds that only the wake potential over the length of the bunch is of interest. This implies that, in the frequency domain, the bunch cannot resolve the details of the sharp resonances of the cavity and it rather experiences an average effect. The impedance function is usually described by the so-called "broad-band (BB) resonator impedance" which replaces the set of parasitic modes of the cavity [24]:

$$Z^{BB}(\omega) = \frac{R_s^{BB}}{1 + j\left(\frac{\omega}{\omega_r} - \frac{\omega_r}{\omega}\right)} \qquad (52)$$

The BB shunt impedance R_s is estimated by averaging the resistive part of the parasitic resonance of the cavity (which can be measured by means of the perturbation method, or estimated by computer codes) to give the same energy loss as the whole cavity. Because of Eq.(6), each resonance contributes with only half the area of its spectrum [24-25]:

$$R_s^{BB} = \frac{\pi}{4} \sum_n \omega_n \left(\frac{R}{Q}\right)_n \qquad (53)$$

The quality factor in eq.(52) has been taken as Q=1, while the resonant frequency is $\omega_r = \omega_{cut\text{-}off} = 2.4(c/b)$, i.e. the frequency cut-off of the cavity-pipe iris (these choices are arbitrary). The effect of the various discontinuities in the vacuum chamber are also usually included in those of the BB resonator [24].

The transverse BB impedance resonator is obtained from the longitudinal one by using the approximate relation:

$$Z_\perp^{BB}(\omega) = \frac{2c}{b^2} \frac{Z^{BB}(\omega)}{\omega} \qquad (54)$$

The main advantage of the BB model is its simplicity which facilitates evaluation of stability limits and growth rates and comparison with measurements. However the BB resonator model has some limitations expecially

for very short bunches where the high frequency impedance behaviour is of great importance. In fact the BB resistive asymptotic frequency dependence is ω^{-2} while analytical studies have predicted a $\omega^{-1/2}$ for a single cavity and $\omega^{-3/2}$ for periodic cavities. An improved impedance model has been recently developed [26].

3.2 LOW INTENSITY REGIME : STATIONARY DISTRIBUTION

The longitudinal motion of a single particle within a stationary bunch, in the presence of additional focusing or defocusing forces induced by the bunch itself is described by the following equation [6,8]:

$$\ddot{\tau} + \omega_{so}^2 \tau = \frac{-\eta\, e\, I_b}{2\pi R(E/c)} \int_{-\infty}^{\infty} Z(\omega)\; h_o(\omega)\; e^{j\omega\tau}\, d\omega \qquad (55)$$

where $h_o(\omega)$ is the normalized current distribution, I_b the bunch current, τ is the position of the particle with respect to the synchronous one, η is the common phase-slip factor ($\alpha_c - 1/\gamma^2$), R is the machine radius, E the particle energy, and ω_{so} the incoherent unperturbed synchrotron frequency. The driving term is the average longitudinal force given by Eq. (25). Because of the motion periodicity the spectrum of a stationary bunch is given by a set of impulsive lines at frequencies which are a multiple of the revolution frequency $f_o = 2\pi\omega_o$; for example in the case of a gaussian distribution we have [8]:

$$I(\omega) = I_b\, h_o(\omega) = I_b \sum_p \delta(\omega - p\omega_o)\, \exp\left[\frac{-(p\omega_o\sigma_\tau)^2}{4}\right] \qquad (56)$$

If the most significant lines of the bunch spectrum, i.e. those before the exponential roll-off, are such that $p\omega_o\tau << 1$ (condition which is easily satisfied by long bunches), the exponential term in Eq. (55) can be expanded in series retaining the first terms:

$$\ddot{\tau} + \omega_{so}^2 \tau = \frac{-\eta\, e\, I_b}{2\pi R(E/c)} \left[\int_{-\infty}^{\infty} Z(\omega)\, h_o(\omega) \left[1 + j\omega\tau - (\omega\tau)^2 \right] d\omega \right] \qquad (57)$$

Analysis of the above equation [8] shows that the stationary self field induces the following effects:

- additional losses in the resistive walls and in the parasitic HOM, (resistive impedance) which change the synchronous phase.

- an additional off-phase voltage which modifies the external r.f. slope (potential well) and therefore the incoherent synchrotron frequency and bunch-length due to the imaginary impedance.

- spread of the synchrotron frequency due to the non linear term which make the frequency shift dependent of the amplitude oscillation τ.

3.2.1 Synchronous phase shift

The synchrounous particle phase shift is [2-9]:

$$\Delta\phi_s = \omega_{rf}\tau_s = \frac{I_b}{V_{rf}\cos\phi_{so}} \int_{-\infty}^{\infty} Z_r(\omega)\, h_0(\omega)\, d\omega \qquad (58)$$

where ω_{rf} is the r.f. angular frequency, V_{rf} is the r.f. peak voltage, ϕ_s is the synchronous phase. The r.f. voltage supplies the additional energy per turn lost by the bunch in the resistive impedance.

The total energy per charge supplied by the r.f. system is related to the new synchronous phase by:

$$U = eV_{rf} \sin \phi_s \qquad (59)$$

In order to measure the energy loss U and the synchronous phase ϕ_s we may compare the phase of the r.f. signal to a pick-up signal filtered at the same frequency ω_{rf} [27,28] as shown in Fig.15.

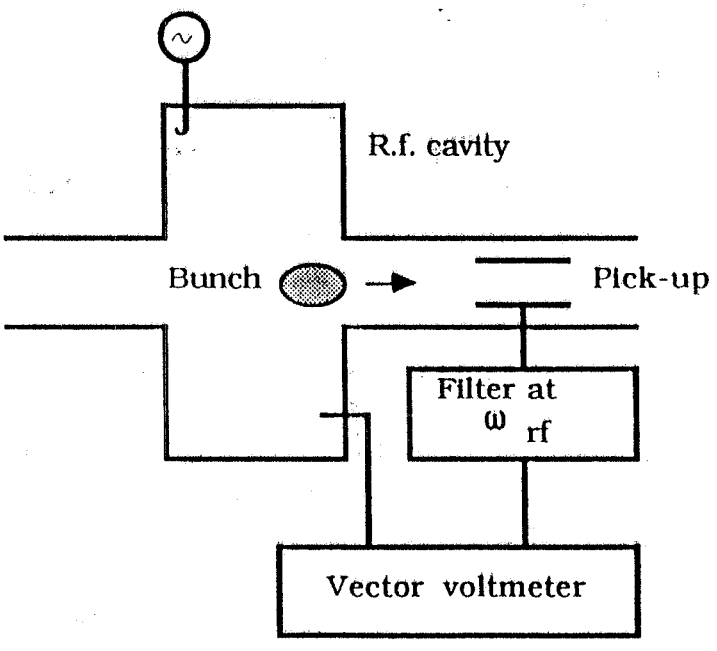

Fig. 15 Synchronous phase shift measurement

By measuring ϕ_s at different current values one can draw a curve of the type shown in Fig. 16 obtained for the SLAC Damping Ring [28].The graph is obtained by displaying the relative phase $\Delta\phi_s$ measured while the beam current is reduced by means of a scraper.

In the stationary regime (low current) the bunch distribution does not change, therefore according to Eq. (58) the phase shift is a linear function of the current.

It is apparent that this measurement gives only global information about the resistive impedance. More information can be derived from the loss factor k whose dependence on the bunch-length is straigthforward related to the frequency dependence of the resistive impedance, as stated in Eq.(28). The loss factor can be determined from the slope of the the phase shift curve and is given by:

$$\frac{\Delta\phi_s}{\Delta I_b} = \frac{1}{f_0 V_{rf}} k(\sigma_\tau) \qquad (60)$$

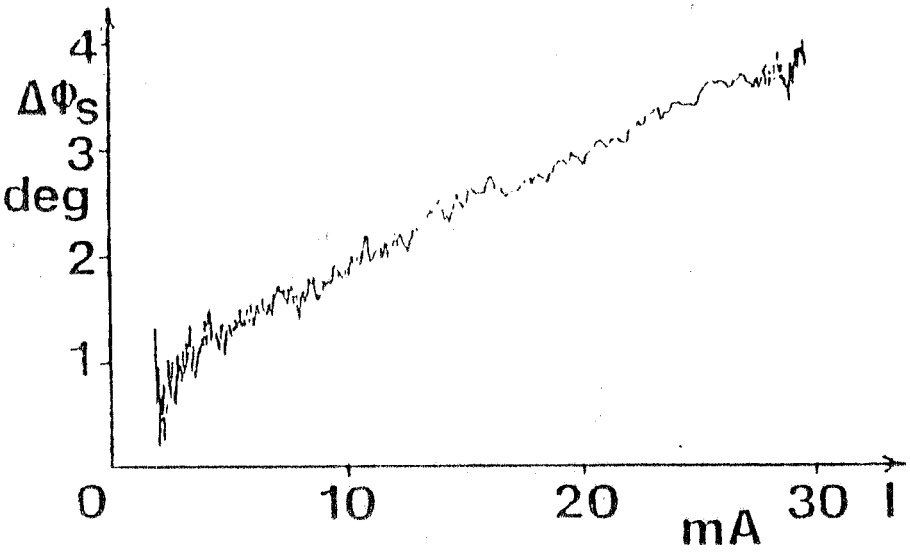

Fig.16 - Synchronous phase measurement at SLAC Damping Ring.

3.2.2 Incoherent frequency shift and potential well distortion

The linear term of Eq. (57) modifies the slope of the effective voltage seen by the bunch of particles and therefore induces a shift of the incoherent synchrotron frequency ω_s given by:

$$\frac{\omega_s^2 - \omega_{so}^2}{\omega_{so}^2} = \frac{I_b}{\omega_{rf} V_{rf} \cos\phi_{s0}} \int_{-\infty}^{\infty} \omega Z_i(\omega)\, h_o(\omega)\, d\omega \qquad (61)$$

Space charge and BB imaginary impedances are linear functions of the frequency and their contribution to the above integral is dominant compared to that of the resistive wall impedance. Since the ratio $Z_i(\omega)/\omega$ remains constant over a wide frequency range which contains the bunch spectrum for not too short bunches, the frequency shift can be written in the form:

$$\frac{\omega_s^2 - \omega_{so}^2}{\omega_{so}^2} = \frac{I_b}{\omega_o \omega_{rf} V_{rf} \cos\phi_{s0}} \left(\frac{Z_i(\omega)}{p}\right)_o \int_{-\infty}^{\infty} \omega^2 \, h_o(\omega) \, d\omega \qquad (62)$$

where, according to Eq.(56), $\omega = p\omega_o$, $(Z_i(\omega)/p)_o$ is the low frequency constant value as plotted in Fig.17, and where the remaining integral can be easily evaluated for a particular bunch spectrum. Below the transition energy $\cos\phi_s > 0$, the synchrotron frequency is decreased by the space charge and increased by BB inductance. The opposite occurs above the transition energy.

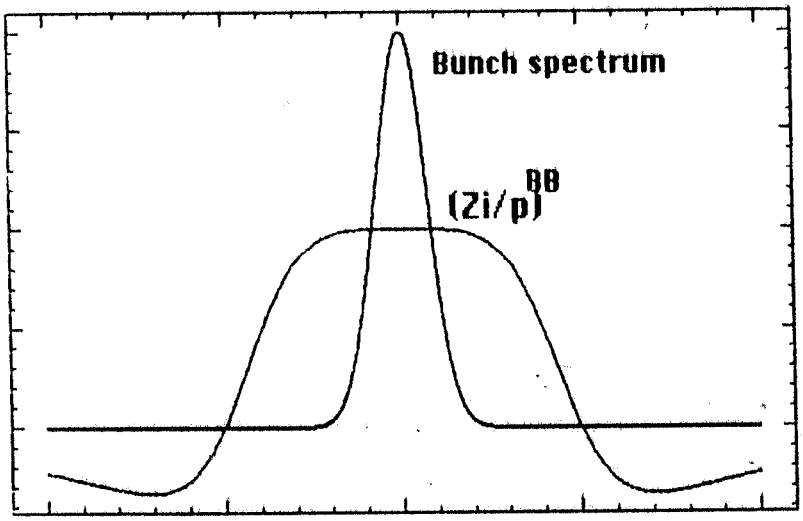

Fig.17 Imaginary BB impedance and bunch spectrum.

Measurement of the incoherent synchrotron frequency would permit an estimation of the imaginary impedance by means of Eq. (62). Unfortunately the intensity of the incoherent signals are covered by the much more intense signals induced by the coherent bunch motion and are therefore difficult to detect.

However we know [3-9] that in the stationary regime the equilibrium bunch length is also affected by the potential well distortion. By including the potential well effect, new equilibrium conditions are derived. For protons (parabolic distribution) requiring the conservation of the longitudinal phase space, we get:

$$\left(\frac{\sigma}{\sigma_o}\right)^4 - \frac{24\pi I_b}{N_h V_{rf}\cos\phi_s}\left(\frac{R}{\sigma_o}\right)^3\left(\frac{\sigma}{\sigma_o}\right)\left(\frac{Z_i(\omega)}{p}\right)_o - 1 = 0 \qquad (63)$$

where σ_o is the unperturbed bunch length and Nh is the harmonic number. For electron bunches with a gaussian distribution whose equilibrium sizes are determined by synchrotron radiation, we have:

$$\left(\frac{\sigma}{\sigma_o}\right)^3 - \left(\frac{\sigma}{\sigma_o}\right) - \frac{\sqrt{2\pi}\, I_b}{N_h V_{rf}\cos\phi_s}\left(\frac{R}{\sigma_o}\right)^3\left(\frac{Z_i(\omega)}{p}\right)_o = 0 \qquad (64)$$

Both Eqs. (63) and (64) are derived assuming a negligible synchronous phase shift [6].

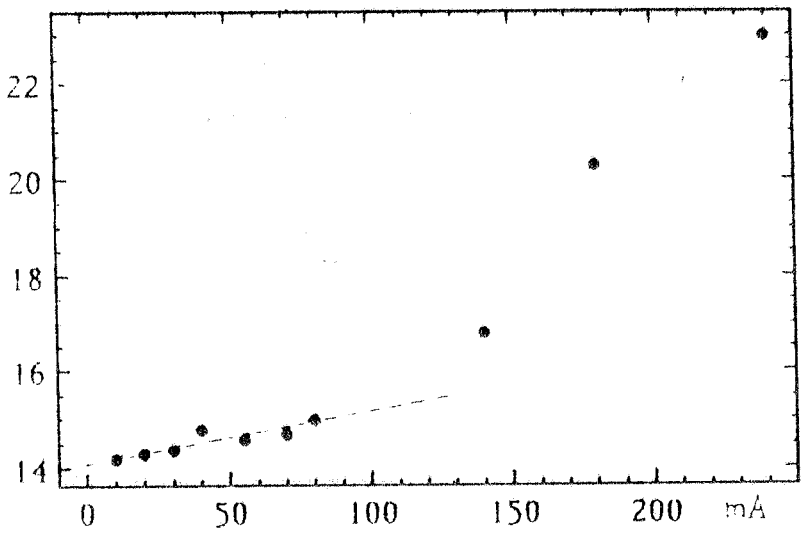

Fig.18 - ISR bunch length measurements.

Fitting bunch-length measurements data in the low current regime with Eqs. (63) or (64) yields an estimation of the imaginary part of the impedance. In Fig.18 we report the data of measurements performed at ISR (CERN) [29] from which the imaginary impedance impedance was estimated to be almost 20Ω.

It is worth noting that above a given threshold current the bunch lengthens because of a different mechanism called "turbulence" that will be discussed later. Sometimes this threshold occurs at quite low current intensity and the imaginary part of the impedance can no longer be estimated by means of the potential-well effect alone.

3.3 COHERENT SYNCHROTRON TUNE METHOD

The direct measurement of the incoherent synchrotron frequency is difficult. However, an indirect measurement can be made by observing the single-bunch, coherent, higher-order modes which can be easily detected by means of a longitudinal pick-up. At low current intensity the coherent dipole mode corresponds more or less to an off-centered rigid motion of the bunch in the phase space and therefore oscillates with the same frequency as the incoherent oscillations.

$$f_{s1} = f_{so} = f_o \left(\frac{e\eta \, N_h \, V_{RF} \cos \phi_s}{2\pi \, \beta^2 \, E} \right)^{1/2} \tag{65}$$

Measurement of the coherent dipole mode frequency may be useful to check the measurement conditions and for calibrating the r.f. parameters.

Coherent high-order modes (quadrupole, sextupole etc.) are instead affected by the self-forces since they do not represent rigid bunch motions. Detecting for instance a sideband f_{s2} corresponding to the quadrupole mode, one can observe a line shifted with respect to the unperturbed quadrupole frequency $2f_{so}$ (twice the dipole incoherent frequency) as a function of the current intensity. The magnitude of the coherent frequency shift is related to the incoherent one [8,9]:

$$f_{s2} - 2f_{so} = \mu \, \Delta f_s^{incoh.} \tag{66}$$

The constant μ depends on the bunch distribution [8,9]. In Fig.19 we report the frequency shift of the coherent quadrupole mode measured at the ISR [29] for parabolic bunches for which μ=.5 [30].

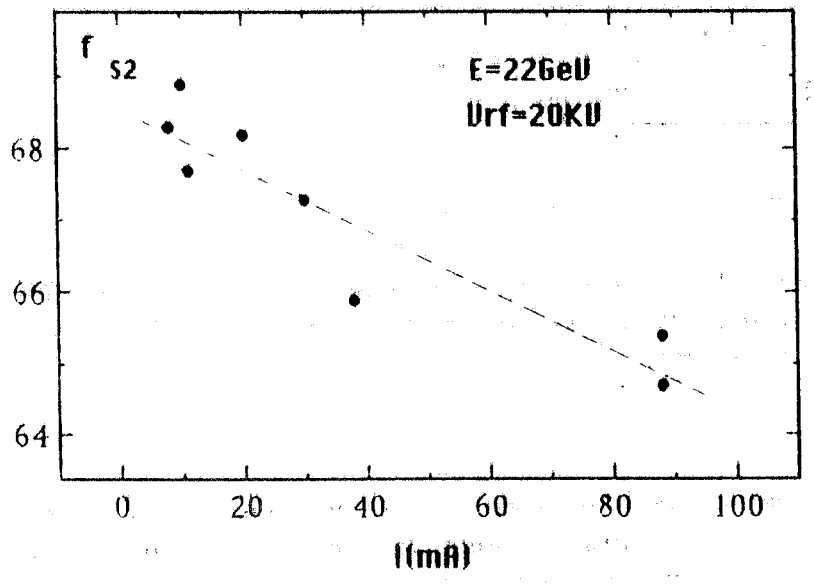

Fig.19 - Coherent quadrupole synchrotron frequency vs. beam current at ISR.

From the slope of the data fit one can determine the effective impedance $(Z_i/p)_o$ sum of the space charge and BB imaginary impedances (See Appendix).

$$\left(\frac{Z_i(\omega)}{p}\right)_o = - \frac{2Z_o}{2\beta\gamma^2}\left[1 + 2\ln\frac{b}{a}\right] + \left(\frac{R_s\,\omega_o}{\omega_r}\right)^{BB} \qquad (67)$$

Measurement of the effective impedance at different energies permits the impedance contributions (SC and BB) to be derived separately [29].

In order to investigate the quadrupole coherent frequency shift it is necessary to excite the quadrupole coherent mode for example by modulating the amplitude of the r.f. voltage at a frequency approximately twice the incoherent synchrotron frequency. A network analyzer is used to observe the longitudinal transfer function . In Fig.20 the basic scheme of these measurements is shown:

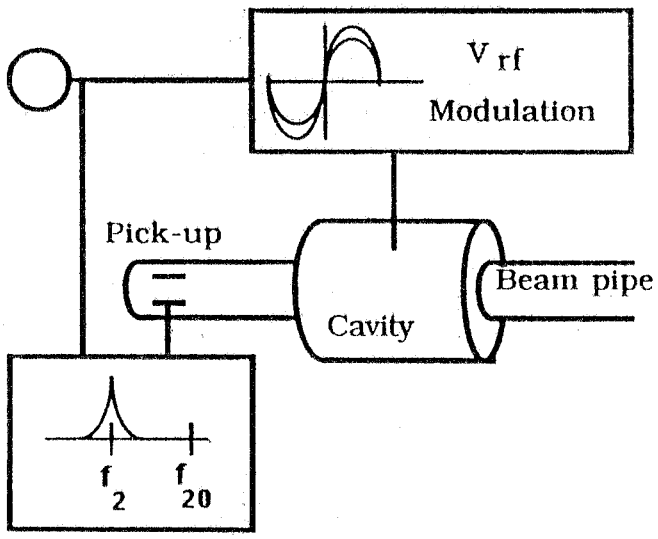

Fig. 20 Measurement scheme of the frequency shift of the quadrupole mode

To exclude other effects producing a similar frequency shift, such as coupled-bunch mode instabilities, these measurements should be performed with only one bunch stored in the machine.

It is worth remarking that an accurate measurement of the frequency shift in any case requires an accurate bunch-length measurement (the incoherent frequency shift depends on the bunch spectrum that is affected by the potential well) from which the impedance can be estimated straigthforwardly.

3.4 HIGH INTENSITY REGIME : MICROWAVE INSTABILITIES.

Above a certain current intensity a new instability mechanism arises. This effect causes the bunch to increase its energy spread and therefore its length. An attempt to explain this effect introduces the coupling between the coherent bunch modes [31, 32]. However, an accurate prediction of the current threshold is given by the Boussard's criterion [33] derived from the Keil-Schnell coasting beam stability criterion [34] by using the local values of current and energy spread σ_E. This model reasonably fits the experimental data. For electrons above the current threshold:

$$I_{th} = \frac{\sqrt{2\pi}\ \alpha_c^2\ |E/e|}{Q_s \left|\frac{Z}{p}\right|}\left(\frac{\sigma_E}{E}\right)^3 \tag{68}$$

where Q_s is the synchrotron tune, the bunch finds new equilibrium conditions:

$$\left(\frac{\sigma_E}{E}\right)^3 = \frac{1}{\sqrt{2\pi}}\frac{Q_s I_b}{\alpha_c^2\ |E/e|}\left|\frac{Z}{p}\right|$$
$$\left(\frac{\sigma}{R}\right)^3 = \frac{1}{\sqrt{2\pi}}\frac{\alpha_c I_b}{Q_s^2\ |E/e|}\left|\frac{Z}{p}\right| \tag{69}$$

For long bunches, the absolute value of the effective BB impedance $|Z/p|$ does not depend on the bunch length σ, see Fig. 21. $|Z/p| \approx (Z_i/p)_o$ since the real impedance $(Z_r/p)_o$ vanishes at low frequencies. Accordingly both momentum spread and bunch length increase with the current with the $I^{1/3}$ law. Actually the bunch length may result from a combination of the potential well and turbulent effects. Including the dependence of the synchrotron tune on the current we get for long bunches [24]:

$$\left(\frac{\sigma}{R}\right)^3 = \frac{\sqrt{2\pi}\ I_b}{N_h\ V_{rf}\cos(\phi_s)}\left\{\left|\frac{Z}{p}\right|_o + \left(\frac{Z_i}{p}\right)_o\right\} \tag{70}$$

where, as already said, $|Z/p|_o \approx (Z_i/p)_o$.

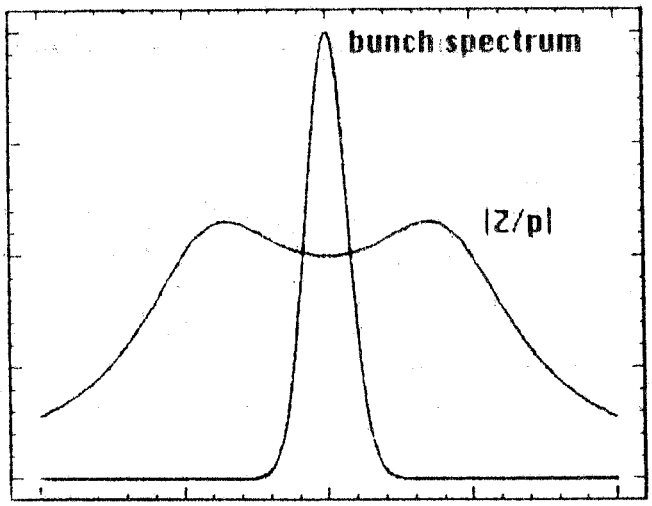

Fig. 21 Gaussian bunch spectrum and absolute BB resonator impedance

In Fig. 22 we report, as an example, the measurements of bunch lengthening at DCI [35]. Fitting the values of the normalized bunch length versus the current $I_b^{1/3}$, one can derive the impedance value directly from the slope of the curve. It is worth remarking that the bunch length depends only on the impedance and on the parameter δ (see Fig. 22) We shall see that this result is quite general.

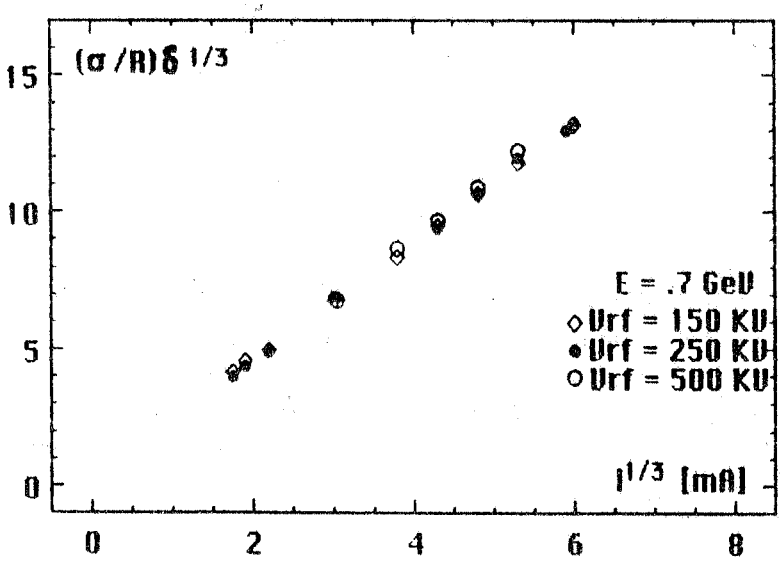

Fig. 22 DCI bunch-length measurement. ($\delta = N_h V_{rf} \cos\phi_{so}/\sqrt{2}\pi$)

Similar measurements at different machines (ADONE, EPA, SPEAR, SLC-DR etc) [36,37,38,39], with bunches sufficiently long, confirm the validity of the above model. The effect of the microwave instabilities on proton bunches can be found in Ref.40 (SPS) and in Ref.41 (ISR).

In the case of bunches shorter than the beam pipe radius, the impedance |Z/p| can no longer be considered constant. In fact the microwave instabilities are caused by e.m. fields whose wavelength is shorter than the bunch length (instability mechanism arising inside the bunch). If the bunch length is shorter than the beam pipe radius, the bunch spectrum covers a frequency region beyond the beam pipe cut-off (see Fig. 23) where the $|Z/p|^{BB}$ impedance is no longer constant and behaves asymptotically as ω^{-2}. In this region the BB impedance model fails and a different model must be applied.

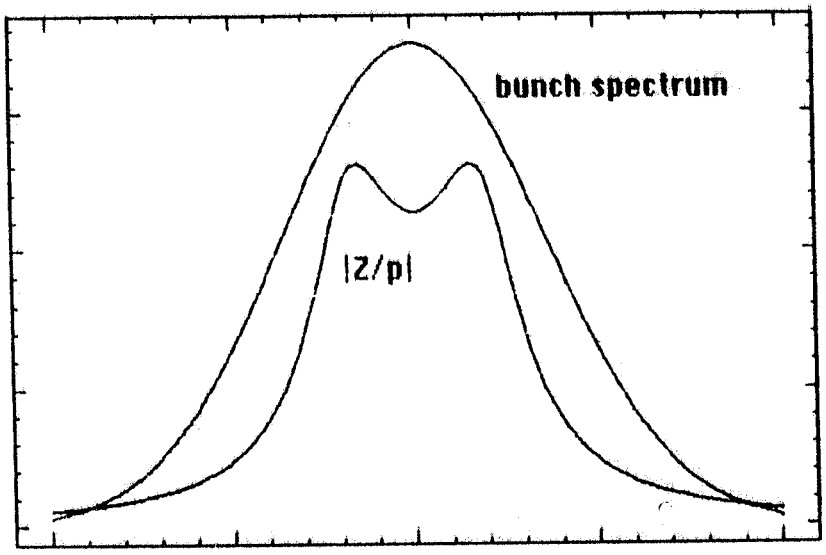

Fig. 23 |Z/p| and short bunch spectra.

Assuming a frequency dependence for the impedance:

$$Z(\omega) = Z_0 \omega^a \text{, namely: } \left(\frac{Z}{p}\right) = \left(\frac{Z}{p}\right)_o \omega^{a-1} \tag{71}$$

A. Chao and J. Gareyte have derived a more general scaling law for bunch lengthening [42]. The bunch length satisfies the scaling property $\sigma = F(\xi)$:

$$\sigma \propto \left(\xi Z_0 R^3\right)^{\frac{1}{2+a}} \tag{72}$$

where R is the machine radius and:

$$\xi = \frac{I_b \alpha_c}{Q_s^2 E} \tag{73}$$

Note that the long-bunch scaling law is re-obtained for a=1, i.e. where |Z/p| is constant. Thus the long-bunch case can be thought of as a particular case of the general law (72). In Fig. 24 we show the experimental data obtained at SPEAR II. The slope of the fit indicates the value a = -.68 in the frequency range above a

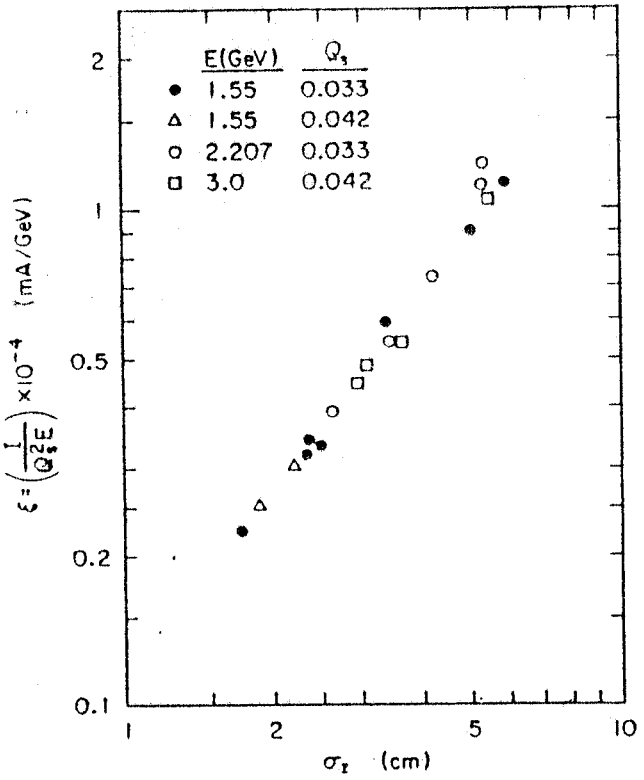

Fig. 24 Scaling parameter ξ as function of σ at SPEAR

Thus in the regime of extremely short bunches, bunch-length measurement permits to derive the high frequency behavior of the impedance.

3.5. ENERGY LOSS OF A COASTING BEAM

It was shown at the ISR [44,45] that the high frequency behavior of the resistive impedance can be derived by observing the energy loss of unbunched proton and antiproton beams. It was observed that the measured energy loss of these beams was larger than expected for interaction with residual gas and for synchrotron radiation, and this was explained by taking into account the parasitic loss due to the wall current induced by individual particles undertaking statistical fluctuations (Schottky noise).

Observed at the wall, the signal induced by an individual particle has an effective r.m.s time length given by:

$$\sigma = \frac{b}{\sqrt{2}\, c\gamma} \tag{74}$$

which is function of the energy. The spectrum of this uncorrelated current signal extends to a frequency $\omega^* = c\gamma/b$ (b = beam pipe radius) which is typical of an individual charge spectrum (for $\beta \cong 1$) [44]:

$$\tilde{I}_w(\omega) = \frac{-e}{\sqrt{2\pi}\, I_0(\omega/\omega^*)} \tag{75}$$

Beyond ω^* the signal disappears because of the exponential behavior of the modified Bessel function $I_0(x)$. The power spectrum of this signal is plotted in Fig. 25.

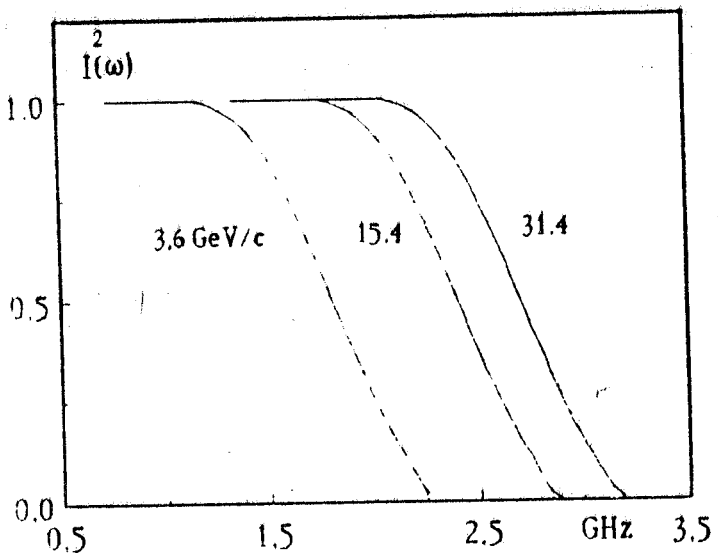

Fig. 25 Wall-current power spectrum.

Since the contributions of the individual particles are uncorrelated, the power of the total signal is the sum of the individual power contributions. Similarly the energy lost by the beam (24) is equal to the sum of the energy lost by each particle:

$$U = 2 \int_0^\infty \tilde{I}_w^2(\omega)\, Z_T(\omega)\, d\omega \tag{76}$$

The signal power spectrum stays almost constant up to the frequency ω^* (see Fig. 25), therefore the loss factor (4) is well approximated by:

$$k(\omega^*) = \frac{U}{e^2} \cong \frac{1}{\pi} \int_0^{\omega^*} Z_T(\omega)\, d\omega \tag{77}$$

It is apparent that measuring k at different energies it is possible, because of Eq. (74), to draw a plot of the loss factor versus the rms pulse length. The data fit

permits the high frequency behavior of the impedace to be derived according to Eq. (28). Deriving the loss factor expression (77) with respect to the frequency yields:

$$Z_r(\omega^*) \cong \pi \left[\frac{\delta k(\omega^*)}{\delta \omega^*}\right] = - \frac{\pi}{\sqrt{2}\,(\omega^*)^2} \left[\frac{\delta k(\omega^*)}{\delta \sigma}\right] \qquad (78)$$

where the impedance is simply related to the local slope of the curve fit. In Fig. 26 we show the energy loss per turn and the parasitic loss parameter as function of the rms pulse length of the wall current measured at ISR. The data fit indicates that at high frequencies the impedance scales as $\omega^{-1/2}$ [45], as predicted for a single resonator.

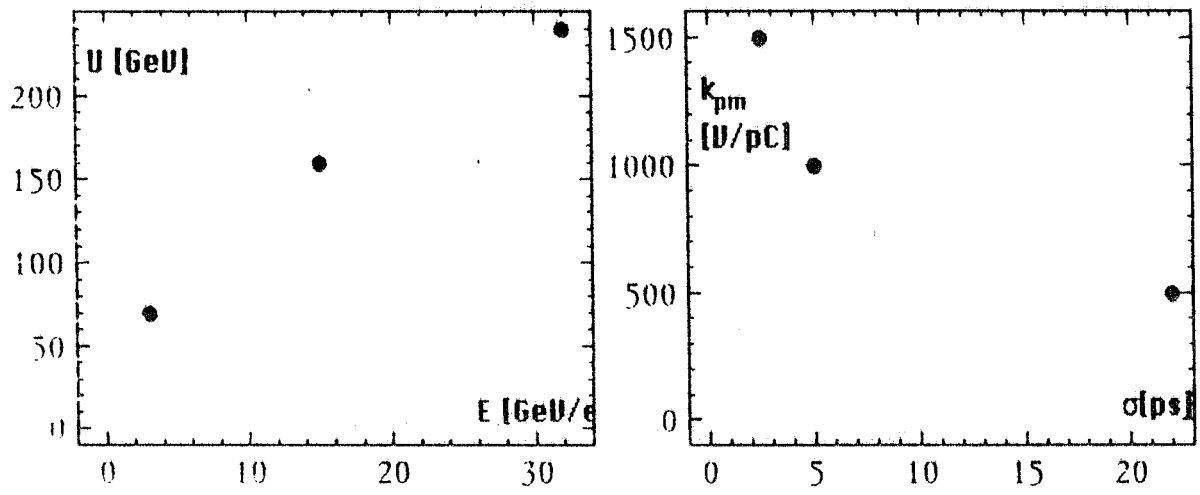

Fig.26 - Energy loss and loss factor versus the pulse length.

The experiment performed at the ISR consists of a careful measurement of the beam orbit radius as function of time, keeping the magnet fields absolutely constant. Without energy recover from r.f., the energy loss leads to a steady decrease of the orbit radius R. The change of R is determined from the revolution frequency which, in turn, is measured by observing at regular time intervals the longitudinal Schottky noise spectrum. The corresponding change in momentum is obtained from the known momentum compaction factor. The radiated loss U_{sr} is subtracted giving the remaining parasitic loss.

3.6 TRANSVERSE IMPEDANCE MEASUREMENTS

We conclude this chapter by briefly describing the main methods adopted for measurements of the transverse impedance: head-tail and transverse coherent mode coupling for bunched beams, coherent-incoherent tune shift method and transverse BTF for coasting beams.

3.6.1 Head-tail growth rate measurements

The growth rate of the head-tail instability [47,48,49] is widely used for estimating the real part of the transverse impedance by comparing the measured growth rate with the theoretical prediction:

$$\frac{1}{\tau} = \frac{-1}{m+1}\,\frac{\beta}{\pi Q_x f_o}\,\frac{e I_b}{4 l_b \gamma m_o}\,Z^m_{\perp,\mathrm{eff}} \tag{79}$$

where l_b is the full bunch length (taken as $l_b = 4\sigma$) and

$$Z^m_{\perp,\mathrm{eff}} = \frac{\int_{-\infty}^{\infty} Z_\perp(\omega)\, h_m(\omega-\omega_\xi)\, d\omega}{\int_{-\infty}^{\infty} h_m(\omega-\omega_\xi)\, d\omega} \tag{80}$$

and h_m is the frequency spectrum of the m-th coherent oscillation made by the bunch. The bunch spectrum of the zero mode is centered at the frequency [49]:

$$\omega_\xi = \frac{\xi}{\eta} Q_x\, \omega_o \tag{81}$$

so that, changing the chromaticity, it provides an excellent probe of the transverse impedance seen by the beam [28,50].

3.6.2 Transverse mode measurements

Analogously to the longitudinal case, analyzed in Sec. 3.3, the transverse self-forces affect the transverse beam dynamics leading to a shift of the transverse coherent modes [49,50,51]. For low current intensity the frequency of the lowest radial modes of m-th order are:

$$f^m_\perp = f_0\left(Q_x + m Q_s\right) \tag{82}$$

where Q_x is the fractional part of the transverse betatron tune and Q_s is the incoherent synchrotron tune.

The betatron tune shift with respect to the zero current value Q_{x0} due to the beam-wall interaction,is:

$$\Delta Q^m_x = \frac{j}{|m|+1}\,\frac{e\,\beta_x I_b}{4\, l_b\, E}\,Z^m_{\perp,\mathrm{eff}} \tag{83}$$

where β_x is the betatron function at the location of the main impedance components, usually at r.f. cavity and kickers, otherwise its average value over the ring [47,48].

In Sec. 3.2.2 we have seen that also the incoherent synchrotron frequency Q_s changes its value according to Eq. (63), because of the potential well effect.

Thus when we display on a network analyzer the sidebands of a coherent transverse mode, we observe a frequency shift due to both betatron and synchrotron tune shifts [52,53]:

$$\Delta f_{\perp}^{m} = f_0 \left(\Delta Q_x^{m} + m \, \Delta Q_s \right) \tag{84}$$

Since the zero mode m = 0 is not affected by the synchrotron motion it permits an estimation of the transverse imaginary impedance. If the bunch power spectrum lies in the low frequency region where the transverse BB imaginary impedance is almost constant, it results that [51]:

$$Im\left(Z_{\perp,eff}^{m}\right) = \frac{R_{\perp}}{Q_{\perp}} = \frac{-4 \, l_b \, E}{e \, \beta_x \, I_b} \, \Delta Q_x^{m=0} \tag{85}$$

Some interesting information is derived by observing the dipole transverse modes m = 1 and m = -1. These modes are characterized by identical betatron tune shifts and opposite synchrotron tune shift contributions. As a consequence the total shifts of these modes are different one from the other and not equal to half the m=0 mode (as expected for negligible longitudinal effect).

Quite interesting conclusions are found by observing that the separate contribution (betatron and synchrotron) can be easily extracted. In fact it is easy to show that:

$$\Delta Q_x^{m=1} = \frac{1}{2f_0} \left[\left(\Delta f_{\perp}^{m=1} \right) + \left(\Delta f_{\perp}^{m=-1} \right) \right] \tag{86}$$

and

$$\Delta Q_s^{incoh.} = \frac{1}{2f_0} \left[\left(\Delta f_{\perp}^{m=1} \right) - \left(\Delta f_{\perp}^{m=-1} \right) \right] \tag{87}$$

These relations are true provided that the transverse effective impedance does not change for modes m = 1 and m = -1. This assumption is strictly valid for zero chromaticity, and reasonable when the current power spectrum covers the low frequency region (bunches sufficiently long).

We find the following interesting results [51]:

- From measurement of the coherent transverse modes it is possible to derive the incoherent synchrotron shift, quite difficult to measure with longitudinal

dynamics observation.

- From Eqs. (62) and (87) the longitudinal impedance can also be estimated.
- It is possible to derive experimentally the relation between incoherent and coherent synchrotron frequency shift Eq. (67), used in sec.3.3, for longitudinal impedance measurements.

3.6.3 Coherent - inchoerent tune shift method

The low frequency part of the transverse impedance has been measured on machines operating with a coasting beam by observing the coherent and incoherent shift of the betatron frequencies, induced by the self-forces [54,55,56].

The impedance is estimated by measuring both the incoherent and coherent betatron tune shifts versus the beam current [57], according to the following relationship:

$$\Delta Q^{coh.} = \Delta Q^{incoh.} + \frac{e I_b}{2 m_o \gamma_o Q_x \omega_o^2} \left(\frac{Z_\perp^{im}}{2\pi R} \right) \qquad (88)$$

3.6.4 Transverse BTF

The response of a beam to a deflecting r.f. signal (r.f. knock-out) is related to the transverse coherent beam stability [58]. Calling $< x >$ the transverse average beam position and G the amplitude of the r.f. excitation, it has been shown that the transverse self-forces induce a shift of the stability diagram $G/<x>$ [59,60,61] which allows the estimation of either the parasitic beam-wall impedance, or the negative (active) impedance introduced by feedback systems.

ACKNOWLEDGMENTS

We wish to thank A. Hofmann, M. Serio and R. Boni for the useful and clarifying discussions, and S. Turner for having revised the manuscript.

APPENDIX

A1. PERFECTLY CONDUCTING PIPE

A point charge travelling with uniform velocity on the axis of an infinite conducting pipe of radius b creates e.m. fields which travel together whith the charge which does not lose energy. At relativistic energies the field becomes very similar to that of a charge moving in the free space in the region limited by the pipe walls. A nearby charge experiences a repulsive force which vanishes as $1/\gamma^2$. The wake potential has the same energy dependence and is an odd function of the time distance τ, i.e. it vanishes on the leading charge and changes sign crossing it. Accordingly the longitudinal coupling impedance is purely reactive and the force is negative (repulsive) in our convention. In order to account for the space charge fields it is necessary to specify the bunch cross-section radius "a". The space charge longitudinal coupling impedance per unit length, in the limit $\omega b/c\beta\gamma << 1$, is:

$$Z(\omega) = -\,j\,\frac{\omega Z_o}{4\pi c(\beta\gamma)^2}\left(1 + 2\ln\frac{b}{a}\right) \;;\; \left[\Omega/m\right]$$

If the charge is displaced transversely with respect to the axis it will experience a deflecting force. The space charge and induced charge transverse impedance is:

$$Z_{\perp}(\omega) = -\,j\,\frac{Z_o}{2\pi(\beta\gamma)^2}\left(\frac{1}{a^2} - \frac{1}{b^2}\right) \;;\; \left[\Omega/m^2\right]$$

A2. PIPE WITH RESISTIVE WALLS

Due to the resistive wall the leading charge loses energy. A trailing charge experiences a repulsive or attracting force depending on its position relatively to the leading charge. Contrary to the previous case the wake does not vanish at high energies where it reaches the constant value

$$w(\tau) = \frac{1}{4\pi\varepsilon_o b}\sqrt{\frac{1}{\pi\sigma Z_o}}\,(c\tau)^{-3/2} \;;\; \left[V/mC\right]$$

This expression is valid only in the region of attracting force, namely at a distance larger than $(b^2/Z_o\sigma)^{1/3}$, practically everywhere.

The longitudinal coupling impedance shows a new term (besides that of a p.c. pipe) given by:

$$Z(\omega) = \frac{(1+j)}{2\pi b}\sqrt{\frac{\omega Z_o}{2c\sigma}} \quad ; \quad \left[\Omega/m\right]$$

where the resistive part accounts for losses, while the imaginary part is positive consistently with the attractive nature of the wake.

The transverse wake and the transverse impedance are given by:

$$w_{\perp}(\tau) = \frac{r_1}{\pi\varepsilon_o b^3}\sqrt{\frac{1}{\pi\sigma Z_o}}\,(c\tau)^{-1/2} \; ; \; \left[V/mC\right]$$

$$Z_{\perp}(\omega) = \frac{(1+j)\,c}{\omega\pi b^3}\sqrt{\frac{\omega Z_o}{2c\sigma}} \quad ; \quad \left[\Omega/m^2\right]$$

Note the interesting relationship between longitudinal and transverse resistive impedance:

$$Z_{\perp}(\omega) = \frac{2c}{b^2}\,\frac{Z(\omega)}{\omega}$$

A3. RF RESONATOR

A point charge crossing a cavity excites all the resonant modes. Each mode is characterized by a resonant frequency ω_n, a quality factor Q_n, and a shunt impedance R_n.

It has been shown that [4,62,63] the wake potential of a resonant cavity can be expressed as the sum of the wakes excited in each mode:

$$w(\tau) = \sum_n w_n(\tau) = 2\sum_n k_n \cos(\omega_n\tau)\exp\left[-\frac{\omega_n\tau}{2Q_n}\right]$$

where k_n, the loss factor relative to the n-th mode, is related to the resonant frequency and to the $(R/Q)_n$ ratio only:

$$k_n = \frac{\omega_n R_n}{4Q_n}$$

In the frequency domain the impedance of a typical resonator corresponding to each resonant mode is :

$$Z_n(\omega) = \frac{R_n}{1 + jQ_n\left(\frac{\omega}{\omega_n} - \frac{\omega_n}{\omega}\right)}$$

Similarly the transverse wake field is expressed as the sum of the transverse modes excited by a point charge crossing the cavity off-axis.

REFERENCES

[1] L. Palumbo, V.G. Vaccaro,"Wake Fields, Impedances and Green's Function", CAS 1985 Advanced Accelerator Physics School Proceedings, S. Turner Editor, CERN 87-03, (1987).

[2] A.W. Chao, "Coherent Instabilities of a Relativistic Bunched Beam", SLAC-PUB 2946, (1982).

[3] P.B. Wilson, "High Energy Electron Linacs: Application to Storage Ring RF Systems and Linear Colliders", SLAC-PUB-2884, (1982).

[4] K. Bane, P.B. Wilson, T. Weiland, "Wake Fields and Wake Field Acceleration" SLAC- PUB 3528, (1984).

[5] B. Zotter, F. Sacherer and A. Hofmann in "Theorethical Aspects of the Behaviour of Beams in Accelerators and Storage Rings", M.H. Blewett Editor CERN 77-13, (1977).

[6] J.L. Laclare, "Introdution to Coherent Instabilities - Coasting Beam Case", CAS 1984 General Accelerator Physics School Proceedings, P. Bryant and S. Turner Editors CERN 85-19, (1985).

[7] B. Zotter,"Collective Effects - General Description", ibidem.

[8] J.L. Laclare, "Bunched Beam Coherent Instabilities", in CAS 1985 Advanced Accelerator Physics School Proceedings, S. Turner Editor, CERN 87-03, (1987).

[9] J.M. Wang, "Modes of Storage Ring Coherent Instabilities", 1985 U.S. Particle Accelerator School Proceedings, SLAC, Stanford, M.Month Editor.

[10] H. Figueroa et al., "Direct Measurement of Beam-Induced Fields in Accelerating Structures", Physical Review Letters, Vol.60, N. 21, p.2144, (1988).

[11] J.C. Slater, "Microwave Electronics", D.Van Nostrand Company, (1950).

[12] L.C. Maier, J.C. Slater, "Field Strength Measurements in Resonant Cavities" , Journal of Applied Physics, Vol.23, p.68, (1952).

[13] R.F. Harrington, "Time Harmonic Electromagnetic Fields", Mc Graw Hill-Book Company, (1961).

[14] Y. Yamazaky, K. Takata, S. Tokumoto, "Measurement of the Longitudinal and Transverse Coupling Impedance of the HOM of the Re-entrant Accelerating Cavity" KEK 80-8, (1980).

[15] F. Caspers, G. Dome, "Precise Perturbation Field Measurements of Resonant Cavities Higher Order Mode Identification" CERN, SPS/85-46, (1985).

[16] D. Tong, "A New Type of Perturbing Object for High Order Mode Measurements in a Resonant Cavity" DESY M-87-06, (1987).

[17] W. Barry, G.R. Lambertson, "Perturbation Method for the Measurement of Longitudinal and Transverse Beam Impedance" LBL-22212, (1987).

[18] M. Sands, J. Rees, "A Bench Measurement of the Energy Loss of a Stored Beam to a Cavity", PEP-95, (1974).

[19] J. Peters, "Bench Measurement of the Energy Loss of a Stored Beam to Vacuum Components", IEEE Trans. NS-24, No.3, p.1446, (1977).

[20] P.B. Wilson, J.B. Styles, K.L.F. Bane, "Comparison of Measured and Computed Loss to Parasitic Modes in Cylindrical Cavities with Beam Ports", SLAC-PUB-1908, (1977).

[21] H. Hahn, F. Pedersen, "On Coaxial Wire Measurements of the Longitudinal

Coupling Impedance", BNL 50870, UC-28, (1978).
[22] F. Caspers, "Beam Impedance Measurement by the Wire Method Using a Synthetic Pulse Technique", IEEE, NS-32, p. 1914, (1985).
[23] G. Lambertson, "Interpretation of the Wire Method of Measuring Beam Impedance below Cutoff", unpublished, (1987).
[24] A. Hofmann, J.R. Maidment, "Current Dependent Phenomena in LEP", LEP Note 168.
[25] K. Hubner, J. Jowett, S. Myers, LEP note 316, (1979).
[26] A. Hofmann, B. Zotter, "Improved Impedance Models for High Energy Accelerators and Storage Rings", CERN LEP/TH 88-51,(1988).
[27] A. Hofmann, 1987 CERN Academic Training Program, , Unpublished.
[28] L. Rivkin et al., "Accelerator Physics Measurements at the Damping Ring", Proceedings of the Particle Accelerator Conference, Vancouver, IEEE NS-32, N.5, p.2626, (1985).
[29] S. Hansen et al., " Effects of Space Charge and Reactive Wall Impedance on Bunched Beams ", CERN/ISR-RF-DI-TH-OP/75-15 (1975) and IEEE Trans. NS-22, No.3, p.1381, (1975).
[30] F. Sacherer,"Methods for Computing Bunched-Beam `instabilities", CERN SI-BR/72-5, (1972).
[31] F. Sacherer, "Bunch Lengthening and Microwave Instability", IEEE Trans. NS-24, No.3, p.1393, (1981).
[32] B. Zotter, " Turbulent Bunch Lengthening and Microwave Instability", IEEE trans. NS-28, No.3, (1981), p.2602.
[33] D. Boussard, CERN/LAB II/ RF/ 75-2, (1975).
[34] E. Keil, W. Schnell, "Concerning Longitudinal Stability in the ISR", CERN/ISR/TH/RF/ 69-48, (1969).
[35] J.C. Denard et al. "Collective Effects on DCI", IEEE Trans., NS-28, No.3, p.2474, (1981).
[36] M. Bassetti et al. "Bunch Length Measurements at ADONE", EPAC Conference, Rome 1988, to be published.
[37] S. Bartalucci and K. Hubner, "Measurement of EPA Bunch Length", PS/LPI Note 87-05, (1987).
[38] M.A. Allen et al., "Some Observation on Bunch Lengthening at SPEAR" , Proceedings IXth Int. Conf. HEA, Stanford, p.352, (1974).
[39] L. Rivkin et al. " Bunch Lengthening in the SLC Damping Ring", SLAC-PUB-4645, (1988).
[40] D. Boussard, J. Gareyte, "Measurements of the SPS Coupling Impedance", SPS/AC/DB/JG/EEK 181, (1980).
[41] P. Bramham et al. "Longitudinal Instabilities of Bunched Beams in the ISR", IEEE Trans. NS-24, No.3, p.1490, (1977).
[42] A.W. Chao and J. Gareyte, "Scaling Law for Bunch Lengthening in SPEAR II", SPEAR-197/PEP-224, SLAC, (1976).
[43] P.B. Wilson et al. "Bunch Lengthening and Related Effects in SPEAR II", IEEE Trans. NS-24, No.3, p.1211, (1977).
[44] A. Hofmann, T. Risselada, "Measuring the ISR Impedance at Very High Frequencies by Observing the Energy Loss of a Coasting Beam", IEEE Trans. NS-30, No.4, p.2400, (1983).
[45] A. Hofmann et al. "The ISR Impedance Between 40 kHz and 40 GHz", IEEE Trans. NS-32, No.5, p.2212, (1985).
[46] A. Hofmann, private communication.

[47] C. Pellegrini, "On a New Instability in Electron Positron Storage Rings : the head-tail effect", LNF 69/45, Frascati, (1969).
[48] M. Sands, "The Head-Tail Effect, an Instability Mechanism in Storage Rings", SLAC-TN-69-8, (1969).
[49] F. J. Sacherer, "Transverse Bunched Beams Instability", Proc. IX Int. Conf. on HEA, (1974).
[50] J. Gareyte, F. Sacherer, "Head-Tail Type Instabilities in the CERN PS and Booster", IEEE Trans., Proc. IX Int. Conf. on HEA, (1974).
[51] B. Zotter, "Transverse Mode Coupling and Head-Tail Turbulence", CERN/ISR-TH/82-10, (1982).
[52] M.P. Level et al. "Transverse Mode Coupling Experiment at DCI", LAL/RT/84-09, (1984).
[53] D. Brandt, J.P. Delahaye, A. Hofmann " Transverse Mode Measurement with positrons in EPA", LEP Note 595 and note PS/LP/87-35, (1987).
[54] L.J. Laslett, 1963 Study on Storage Rings, BNL Report - 7534, (1963).
[55] B. Zotter, CERN Reports ISR-TH/72-8, ISR-TH/74-11 and ISR-TH/74-38.
[56] P. Bryant, "Betatron Frequency Shift due to Self Image Fields", CAS 1986 Second General Accelerator Physics Course Proceedings, S. Turner Editor, CERN 87-10, (1987).
[57] M. Serio, " Betatron Tune Measurements", These Proceedings.
[58] D. Mohl, A.M. Sessler, "The Use of RF-Knock-out for Determination of the Characteristics of the Transverse Coherent Instability of an Intense Beam", Proc. IIX Int. Conference, CERN, p. 334, (1971).
[59] A. Hofmann, B. Zotter, "Measurement of Beam Stability and Coupling Impedance by RF Excitation", IEEE Trans., NS-24, No.3, p.1487, (1977).
[60] J. Borer et al. "Information from Beam Response to Longitudinal and Transverse Excitation', IEEE Trans., NS-26, No.3, p.1487, (1977).
[61] J.Y. Hemery, L. Vos, "A procedure for Obtaining Transverse Wall Impedance and Working Line from Transfer Function Measurements", CERN-ISR-CO-OP/80-32, (1980).
[62] K. Bane and P.B. Wilson, IEEE Trans. NS-24, p.1485 (1977).
[63] T. Weiland and B. Zotter ,"Wake Potentials of a Relativistic Current in a Cavity", Particle Accelerators, Vol.11, p.143, (1981).